

Meterwavelength Single-pulse Polarimetric Emission Survey. V. Flux density, component spectral variation and emission states

RAHUL BASU,^{1,2} DIPANJAN MITRA,^{3,2} AND GEORGE I. MELIKIDZE^{2,4}

¹*Inter-University Centre for Astronomy and Astrophysics, Pune, 411007, India.*

²*Janusz Gil Institute of Astronomy, University of Zielona Góra, ul. Szafrana 2, 65-516 Zielona Góra, Poland.*

³*National Centre for Radio Astrophysics, Tata Institute of Fundamental Research, Pune 411007, India.*

⁴*Evgeni Kharadze Georgian National Astrophysical Observatory, 0301 Abastumani, Georgia.*

Submitted to The Astrophysical Journal

ABSTRACT

We present the flux density measurements of the pulsars observed in the Meterwavelength single-pulse polarimetric emission survey. The average flux densities were estimated in 113 pulsars at two frequencies of 325 and 610 MHz using interferometric imaging. The average profile and single pulse emission in each pulsar were calibrated using the estimated flux density. We have used the flux calibrated average profile to study the variation of the spectral index across the emission beam in 21 pulsars where the core, inner cone and the outer conal components could be clearly identified. The central core component showed a steeper increase in emission at the lower frequency compared with conal emission, with an average difference in spectral index $\delta\alpha_{core-cone} \sim -0.7$ between the core and the conal components in this frequency range. In contrast the inner conal components had positive difference in their spectral index compared to the outer cones with average difference $\delta\alpha_{in-out} \sim +0.3$. The variation in the spectral index across the pulse window should provide valuable inputs for constraining the radio emission processes. The single pulse emission showed the presence of emission mode changing in 12 pulsars with 3 cases where the phenomenon is being reported for the first time. In addition we have also detected enhanced emission for short durations or flaring, in parts or across the entire emission window in 14 pulsars. The sudden changes in the emission during mode changing as well as these bursting states are unrelated to the emission mechanism and suggest the presence of rapid and repetitive changes during the plasma generation process.

Keywords: pulsars:

1. INTRODUCTION

A systematic study of the radio emission properties from normal period pulsars ($P > 0.05$ seconds) has been initiated in the Meterwavelength Single-pulse Polarimetric Emission Survey (MSPES, Mitra et al. 2016). In this survey polarized single pulse emission from 123 pulsars were observed with high detection sensitivity at two frequencies, 325 and 610 MHz, using the Giant Meterwave Radio Telescope (GMRT). Several studies have used this large sample to investigate different emission behaviour, like the average profile polarization behaviour (Mitra et al. 2016), subpulse drifting (Basu et al. 2016; Basu & Mitra 2018a; Basu et al. 2019a), nulling and periodic modulations (Basu et al. 2017, 2020), and period and frequency evolution of the profile component widths (Skrzypczak et al. 2018). In this work we focus on other aspects of the emission behaviour related to the flux density (S), the evolution of the spectral index (α) across the emission beam and state transitions in the pulsar emission. We present a new measurement associated with the MSPES survey, specifically the interferometric estimation of the flux density of the pulsars.

The flux density and the spectral properties provide important inputs into our understanding of the underlying physical processes. The majority of these measurements have been carried out using telescopes comprising of a single dish antenna where the emission is observed with high temporal resolution. The radio emission is usually seen as narrow pulses which occupy around 10% of the period and a stable average profile is obtained after averaging the single pulses. The flux density of the pulsed emission is estimated by characterising the profile baseline level using

the telescope system specifications. There are also estimates of pulsar flux from radio images where the pulsar is seen as an unresolved point source, primarily in large sky surveys (Kaplan et al. 1998; Han & Tian 1999; Kouwenhoven 2000; Frail et al. 2016). In addition interferometric imaging is also used when the profile baselines are affected by the pulsed emission due to scattering and not clearly distinguished (Dembska et al. 2015; Basu et al. 2018). The pulsar emission is affected by scintillation in the intervening medium which can cause strong fluctuations in the flux density over timescales of several minutes to months as well as within the frequency band (Sieber 1982; Rickett 1990).

Pulsars usually show steep power law spectra between 100 MHz and 10 GHz frequency range with an average spectral index of $\alpha \sim -1.6$ ($S \propto \nu^\alpha$, Lorimer et al. 1995; Maron et al. 2000; Jankowski et al. 2018). However, the spectral properties is not uniform across the pulse window. Detailed morphological studies of the pulsar average profile have shown the emission beam to comprise of a central core region surrounded by one or two concentric rings of inner and outer conal emission (Rankin 1990, 1993; Mitra & Deshpande 1999; Mitra & Rankin 2002). A primary distinguishing feature between the core and the conal components within the pulsar profile is the evolution of their respective intensities with frequency. The core component has increasing intensity at lower frequencies suggesting a steeper spectra compared to the cones (Rankin 1983), but very little work has been done to characterise the exact nature of these variations. One notable exercise to understand the spectra of the individual components within the profile was carried out by Kramer (1994), and did not show any clear difference between different components. In this work the profiles were approximated with upto five separate Gaussian functions which were identified as components. This made it difficult to have a direct connection between the core and conal emission and the fitted Gaussian components which were often displaced from the profile components. The large sample in MSPES, with many profiles having both core and conal emission, provided an unique opportunity to explore their relative spectral evolution at the observing frequencies.

The single pulse emission also exhibit variability over multiple timescales due to intrinsic phenomena like mode changing, nulling, subpulse drifting, etc. We have addressed the effects of nulling and subpulse drifting in the MSPES sample in earlier works and explore the mode changing behaviour here. In certain pulsars radio emission properties switches between two or more distinct emission states and the phenomenon is known as mode changing. The most common form of mode changing involve change in the average profile, which assume different shapes in each mode. This phenomenon was first discovered in PSR B1237+25 by Backer (1970a), which switched between a normal and an abnormal mode. Other prominent examples of this behaviour was seen in PSR B0329+54 with four distinct modes (Lyne 1971; Chen et al. 2011), B0823+26 with the Bright and the Quiet modes lasting for hours at a time (Sobey et al. 2015; Hermsen et al. 2018; Basu & Mitra 2019; Rankin et al. 2020), B1822-09 with the Bright mode showing periodic amplitude modulation and a Quiet mode, switching within minutes timescales (Fowler et al. 1981; Backus et al. 2010; Latham et al. 2012; Hermsen et al. 2017), etc. The profile mode changing takes place rapidly, usually within a rotation period of the pulsar, however the average profile shape in the individual modes are highly stable and the pulsar can continue to reside in a particular mode over timescales of minutes to hours. In other cases the mode changing is seen when the subpulse drifting behaviour is transformed in the different modes. The examples of subpulse drifting associated mode changing include the pulsar B0031-07 which shows the presence of three distinct drift modes with different periodicities (Huguenin et al. 1970; Vivekanand & Joshi 1997; Smits et al. 2005; McSweeney et al. 2017), PSR B0943+10 shows the presence of a drifting Bright mode and a non-drifting Quiet mode (Backus et al. 2010; Hermsen et al. 2013), the three drifting modes and one non-drifting state seen in B2319+60 (Wright & Fowler 1981; Rahaman et al. 2021), amongst others. Other forms of mode changing involve transition between a normal emission state and a bursting emission state similar to an RRAT emission, as seen in PSR J1752+2359 (Lewandowski et al. 2004), B0826-34 (Esamdin et al. 2005, 2012), B0611+22 (Seymour et al. 2014; Rajwade et al. 2016), as well as presence of flaring events preceding the pulse window as seen in PSR B0919+06 and B1859+07 (Rankin et al. 2006; Wahl et al. 2016; Han et al. 2016).

We have estimated the flux densities in 113 of the 123 pulsars observed in MSPES by making detailed images of these sources from the interferometric data, which were recorded in conjunction with the high time resolution phased-array observations. The estimated flux densities were subsequently used to calibrate the intensity level of the single pulse emission as well as the average profile. We have investigated the spectral evolution of the core and the conal emission in 21 pulsars where both components were present and could be clearly separated. We have searched for the presence of mode changing in the single pulse emission and found 12 pulsars exhibiting this behaviour, with 3 pulsars where this was seen for the first time. We have also characterised an unique emission behaviour where either in parts or the entire pulse window the intensity is enhanced. This lasts for short durations, usually a single period and was seen

Table 1. Calibrators used in Imaging

325 MHz Observations				610 MHz Observations			
Flux Cal	Flux	Phase Cal	Avg. Flux	Flux Cal	Flux	Phase Cal	Avg. Flux
	(Jy)		(Jy)		(Jy)		(Jy)
3C147	54.0	0025-260	24.7	3C147	39.0	0025-260	14.5
3C286	26.4	0116-208	11.5	3C286	21.7	0116-208	8.1
3C353	153.4	0318+164	8.4	3C48	30.1	0318+164	9.4
3C48	43.9	0323+055	7.3			0521-207	4.4
		0521-207	8.9			0521+166	13.7
		0521+166	15.6			0706-231	6.1
		0804+102	5.6			0804+102	3.5
		0837-198	12.0			0837-198	5.8
		1021+219	6.1			1021+219	3.0
		1033-343	4.8			1033-343	3.4
		1156+314	5.3			1154-350	9.5
		1311-222	16.7			1311-222	8.9
		1510-057	7.4			1330+251	8.2
		1625-311	3.3			1510-057	3.4
		1822-096	3.6			1625-311	2.4
		1830-360	20.7			1714-252	5.5
		1924+334	6.5			1822-096	6.5
		2047-026	6.1			1830-360	16.1
		2137-207	8.3			1924+334	6.3
		2225-049	16.8			2047-026	4.2
		2251+188	7.9			2137-207	7.0
						2219-279	4.6
						2251+188	4.0

in 14 pulsars of this sample. In section 2 we present the details of the interferometric observations and the image analysis used to estimate the average pulsar flux. Section 3 presents the estimated flux density and the details of the single pulse and average profile intensities. We have carried out a detailed estimate of the spectral evolution across the different profile components in section 4. The mode changing behaviour is addressed in section 5, while section 6 characterises the short duration bursting emission. We conclude the paper with a short discussion of the results in section 7.

2. OBSERVATION & ANALYSIS

The GMRT consists of an Y-shaped array of 30 antennas of 45 meter diameter, with 14 antennas located within a central one square kilometer area and the remaining 16 antennas placed along the three arms which has a maximum distance of 27 kilometers. The MSPES observations were carried out at two different frequencies centered around 325 MHz and 610 MHz with a bandwidth of 16.67 MHz at each frequency. The pulsars were observed simultaneously in the ‘phased-array’ mode and the ‘interferometer’ mode. In the phased-array mode the signal from each antenna was co-added in phase to generate high time resolution data (around 0.5 milliseconds) with four polarizations. A bright phase calibrator near the pulsar was observed before the start of the observations to correct for arbitrary phase shifts in each antenna. The time series observations from each pulsar were converted to a series of single pulses, averaged over the frequency band, after correcting for dispersion delays due to propagation in the interstellar medium and removing terrestrial radio frequency interference (RFI). The details of the analysis for obtaining the single pulse sequence from each pulsar is described in [Mitra et al. \(2016\)](#) and [Basu et al. \(2016\)](#). In the interferometric mode the cross-correlated visibility from each antenna pair, called a baseline, was estimated which measured the different

angular scales of the intensity pattern within the field of view of the telescope. The GMRT with 30 antennas can measure visibilities from 435 baselines simultaneously in a co-ordinate system known as the uv -plane. The uv -plane gets filled up due to earth's rotation, which is known as aperture synthesis, and an image of the observed sky intensity distribution is obtained after adding the visibilities from a sufficiently filled uv -plane in their Fourier domain. Similar to the phased-array observations, bright nearby calibrators were observed at regular intervals to address the amplitude and phase variations in the antenna response. In the phased-array observations the measured signal had a baseline level which was a sum of the antenna systematics (T_{sys}) as well as the sky background level (T_{sky}). In contrast the cross-correlation ensured that the mean background level of the images from the interferometer was at zero, and the systematic fluctuations were reflected in the noise rms. As a result it was more reliable to estimate the flux density of the sources from the interferometric images.

The observations were carried out between February, 2014 and July, 2014 over several sessions lasting usually 8-10 hours at a time. Standard flux calibrators 3C147, 3C48 and 3C286 were used during each observing session to estimate the flux scale. On one occasion the non-standard calibrator 3C353 was also used due to the absence of the others within the observing window. These were used to calibrate the flux levels of the phase calibrators which were nearby the intended source and were observed for short durations of 1-2 minutes before and after each pulsar observation. Table 1 lists all the flux and phase calibrators used during these observations. The image analysis were carried out following standard imaging techniques using Astronomical Image Processing System (AIPS). The flux levels of the flux calibrators at each observing frequency were obtained from Perley & Butler (2017) and are listed in table 1. The same phase calibrators were used for multiple nearby pulsars over different observing sessions and their average flux densities are also shown in table 1. In around 10-20 percent of times at either frequency it was not possible to estimate the flux levels of the phase calibrators independently, due to unavailability of any flux calibrator within the observing duration, and the average flux level was used for calibrating the pulsar intensity. The details of the calibrators used during each observing session and the names of the corresponding pulsars they calibrated are reported in table 5 in appendix. The flux levels of the phase calibrators over different observing sessions showed variations that were within 10 percent of the mean level, which served as a consistency check for the flux calibration process. We were primarily interested in the flux measurement of pulsars which were unresolved point sources at the spatial resolutions of GMRT, $8'' \times 8''$ at 325 MHz and $4'' \times 4''$ at 610 MHz, and had contributions at all baselines. A low baseline cutoff of 2 k λ in the uv -range was applied with only higher baselines used for imaging process to reduce the effect of RFI which mostly affected shorter baselines. In some cases the pulsar intensity was affected by scintillation, that introduced phase errors around the source and increased noise rms.

3. AVERAGE FLUX DENSITY AND CALIBRATING THE PULSED EMISSION

The image analysis was carried out in 113 pulsars, with 94 pulsars measured at 325 MHz, 97 pulsars at 610 MHz and 78 pulsars at both frequencies. The average flux densities measured from the maps are listed in table 2, along with the noise rms levels around the pulsar. An example of the contour image corresponding to PSR B0450-18 is shown in figure 1a, where the pulsar is seen as an unresolved point source in the center. There were seven pulsars from the MSPES list where interferometric measurements were not carried out, while an additional three pulsars J0905-4536, B1325-43, and B1634-45 were not detected in the images. The duration of observations varied depending on the pulsar period, with around 2100 single pulses observed in each case. The noise rms in the maps were between 0.2 - 11 mJy at 325 MHz with the typical value around 1 mJy. At 610 MHz the noise levels varied between 0.1 - 3 mJy and usually were around 0.5 mJy. The pulsars were mostly observed on a single occasion at either frequency. However, there were issues with the instrumental setup for single pulse polarization at the lower frequency which required re-observations in around 25 % times (23 cases) at 325 MHz. In addition the two pulsars B0950+08 and B1929+10 were used as polarization calibrators with one or both observed during each observing session. PSR B0950+08 was observed on 6 separate days for a total of 7 different measurements at 325 MHz and had 4 different measurements across same number of days at 610 MHz. The pulsar B1929+10 was observed on 10 observing sessions for a total of 12 different measurements at 325 MHz and on 8 sessions for a total of 12 measurements at 610 MHz.

The pulsar observations were affected by scintillation with diffractive scintillation dominating for pulsars with low dispersion measure which was the case for the majority of the sample (Rickett 1990). We estimated the approximate modulation index for the pulsars in our sample, over the observing durations and bandwidths, from the galactic free electron density model of Cordes & Lazio (2002), which were more than 1 in almost all cases. As a result the measured flux densities of the pulsars, as shown in table 2, can show large deviations from the previously reported values in the

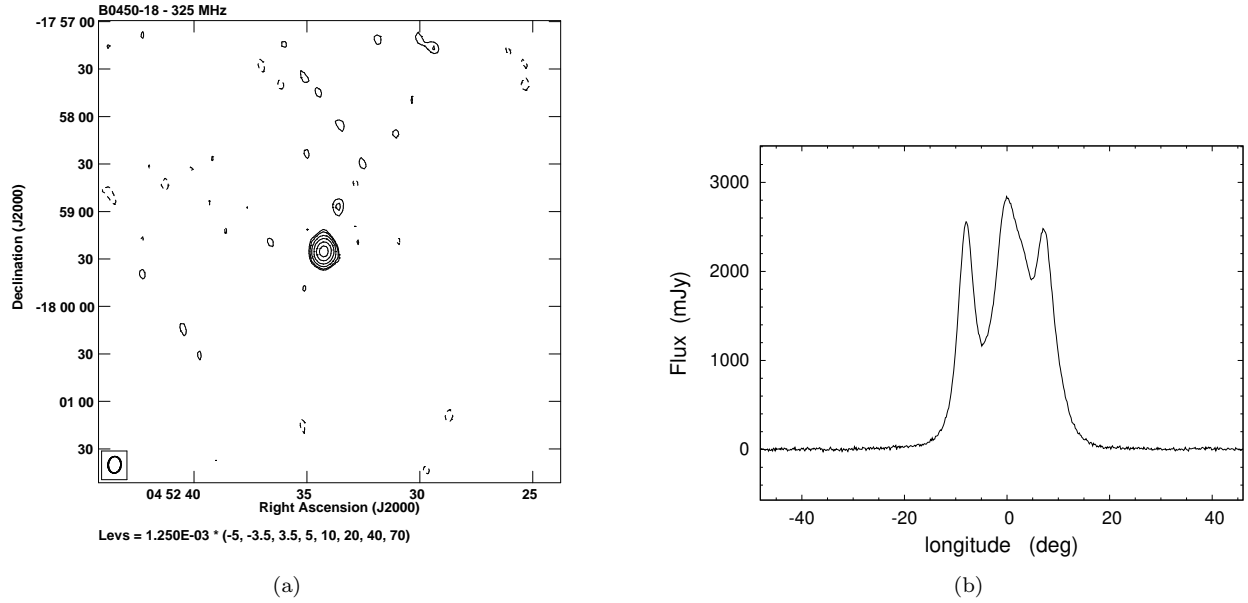


Figure 1. (a) The contour image of the field containing the pulsar B0450-18 at 325 MHz, where the contour levels (Levs) are in units of Jy. The pulsar is seen as a point source in the field center with an estimated flux density of 124.9 ± 5.0 mJy. The synthesized beam corresponding to the spatial resolution of the telescope is shown in the bottom left corner. (b) The average pulsar profile with three distinct components, where the intensity levels have been calibrated using the average flux density from the image. The flux density of the profile peak is 2841 mJy.

literature. This is further highlighted in the case of PSR B0950+08 and B1929+10 which were observed on multiple occasions and showed large variations. For example PSR B1929+10 had flux densities between 70 to 390 mJy at 325 MHz over the different observations. Due to the expected flux variability we have not carried out any absolute spectral index measurements from these observations.

The images measure the average flux over the duration of the observations. When the profile baseline mean level is at zero, the period averaged intensity is equivalent to the flux density measured from the images. As a result once the baseline level is appropriately subtracted from the profile, a scaling relation can be obtained for the measured counts in the phased-array. The pulsar profile was calibrated in all cases where the flux density was available. The single pulse intensities were also calibrated to their flux levels. An example of the flux calibrated profile of PSR B0450-18 at 325 MHz is shown in figure 1b, where the average flux was 124.9 ± 5.0 mJy and the profile had a peak flux level of 2.8 ± 0.1 Jy. The peak flux level was much higher than the average flux since the pulsed emission is only seen for a narrow window ($\sim 10\%$) of the period. The flux levels of the profile peaks are reported in table 2.

The MSPES studies were primarily concerned with the single pulse behaviour of older and middle aged pulsars with characteristic ages of 10^6 years and older. These are mostly isolated pulsars that have moved away from the progenitor supernova remnant, most of which is likely to be dissipated. We have searched for the presence of extended sources within a 20 arcminutes radius of the central pulsar. We found five pulsars with interesting emission features as shown in figure 2. We briefly describe below the nature of the emission from these sources. It should be noted that due to the $2 \text{ k}\lambda$ cutoff in the uv -plane the images were not sensitive to detect large extended structures with size in excess of 5 arcminutes at 325 MHz.

B0656+14 : An extended emission feature was seen below the pulsar which had been identified as a pulsar wind nebula in previous studies (Cordova et al. 1989). However, no clear connection could be made between this extended source and the pulsar (Becker et al. 1999). The emission was broadly divided into two parts, a triangular structure with a bright head, resembling a bow shock, located around 85 arcseconds below the pulsar and a narrow tail ending in a bright point like structure which maybe an unrelated background source. The separation between the bright regions at the head and tail of the source was around 105 arcseconds. The flux density of the extended emission at 325 MHz was 167.5 mJy with the point source at the end of the tail having flux density of 34.3 mJy. The tail connecting

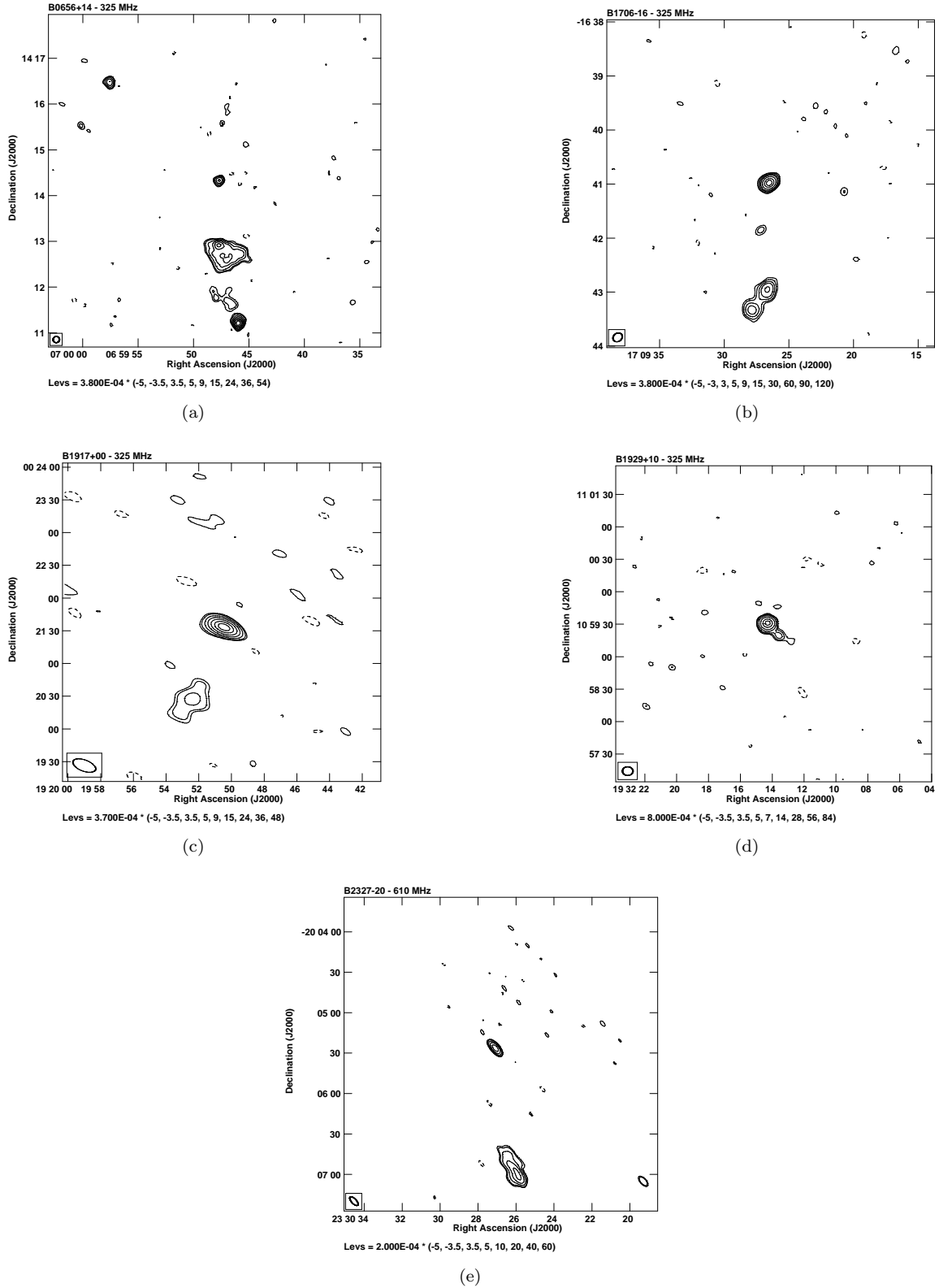


Figure 2. The figure shows the fields of pulsars with interesting sources in their immediate environment. The total intensity contour levels (Levs) are plotted in units of Jy and the pulsar is seen as a point source in field center. The telescope resolution is shown as the synthesised beam in the bottom left corner, and is around $8'' \times 8''$ at 325 MHz and $4'' \times 4''$ at 610 MHz. (a) PSR B0656+14 at 325 MHz. (b) PSR B1706-16 at 325 MHz. (c) B1917+00 at 325 MHz. (d) B1929+10 at 325 MHz. (e) B2327-20 at 610 MHz.

the point source at the end to the main body was not seen at 610 MHz. The extended emission had flux density of 62.9 mJy at 610 MHz while the point source at the end had flux density of 21.6 mJy.

B1706-16 : An extended double lobed structure was seen at a distance of around 120 arcseconds below the pulsar. The extended emission had physical size of around 20 arcseconds and flux density at 325 MHz was 58.4 mJy. The interferometric observations were not carried out at 610 MHz for this pulsar.

B1917+00 : An elongated diffuse emission feature was detected at both frequencies near the bottom left of the pulsar and pointing towards it. The nearest detectable emission was at a distance of 51 arcseconds from the pulsar at both frequencies. The emission was only partially seen at 325 MHz due to the higher noise levels in the map and was between 30-40 arcseconds in size. The total flux density was around 8.9 mJy. At 610 MHz the emission had physical extent of 55-60 arcseconds and the estimated flux density was 9.2 mJy.

B1929+10 : The presence of a diffuse elongated tail opposite to the transverse motion of the pulsar had been reported in previous studies. These detections were primarily in X-rays with no clear counterparts seen at radio wavelengths (Wang et al. 1993; Becker et al. 2006). The primary difficulty with detecting diffuse radio emission in the vicinity of this source is the inherently high flux density of the pulsed emission which makes the noise levels around the source high due to phase errors. The pulsar was used as a polarization calibrator and observed multiple times at both frequencies. However, due to the large flux density of the pulsar it was not possible to detect any clear diffuse emission associated with it on most days. On one or two occasions when the pulsar flux was lower due to scintillation, the elongated tail could be seen (see figure 2d). The tail was seen upto a distance of around 16.5 arcseconds from the pulsar and had flux density of around 16.3 mJy at 325 MHz. On visual inspection it seemed that the orientation of the tail roughly matched the X-ray counterpart. No clear measurements were possible at 610 MHz.

B2327-20 : An elongated source was seen below the pulsar at a distance of around 90 arcseconds. The extended structure was roughly elliptical in shape with major axis of around 32 arcseconds and a minor axis of 16 arcseconds. The estimated flux density was around 39.4 mJy at 610 MHz. Interferometric measurements of this pulsar was not carried out at 325 MHz.

4. SPECTRAL EVOLUTION ACROSS THE EMISSION BEAM

The empirical theory of pulsar emission provides a framework for interpreting the radio emission beam, which comprises of a central core emission surrounded by two concentric rings of inner and outer cones (Rankin 1990, 1993; Mitra & Deshpande 1999). There are other competing models for the emission beam like the patchy beam (Lyne & Manchester 1988), the hybrid patchy-conal beam (Karastergiou & Johnston 2007), the fan beam (Dyks et al. 2010; Wang et al. 2014), amongst others. However, the core-cone model is most widely used in the literature with a wide variety of observational applications. The observed profile shape in this model depends on the line of sight (LOS) traverse across the emission beam and in case of more central cuts, where the LOS passes close to the magnetic axis, profiles with both core and conal components are seen. One primary difference reported in the behaviour of the different component types is their spectral difference, with the core expected to have a steeper spectra compared to the conal components. We intend to estimate the spectral variations across the emission beam from the MSPES sample within the observed frequency range of 325 and 610 MHz. The primary profile types of interest for these estimates are as follows :

- a. Triple (T) which is a three component profile with a central core and one pair of conal emission around it. In some cases one of the conal outriders maybe missing and the pulsar is classified as $T_{1/2}$.
- b. Conal Triple (${}_cT$) and conal Quadruple (${}_cQ$) comprising of three/four component profiles corresponding to the inner and outer cones.
- c. Multiple (M) with five components where the central core component is surrounded by two pairs of inner and outer cones. Figure 3 shows an example of a M type profile in PSR B1857-26.

It is not possible to obtain absolute spectral index of the components as the pulsar emission is affected by scintillation. However, the scintillation are expected to affect the emission across the entire profile in a similar manner. Hence, the

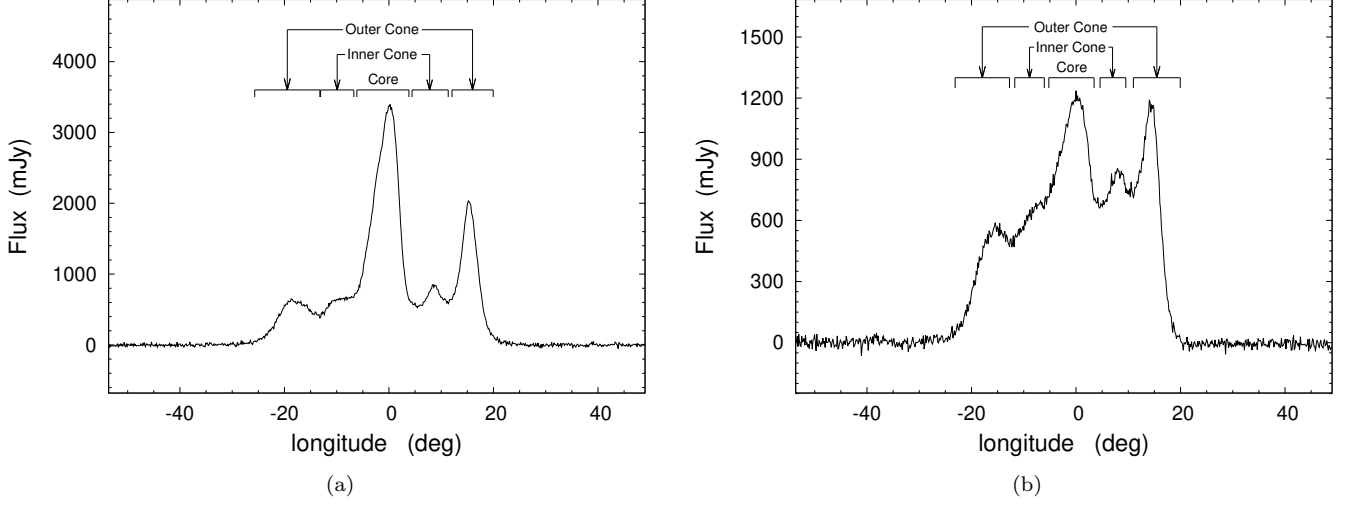


Figure 3. The figure shows the average profile of PSR B1857–26 with five components at (a) 325 MHz and (b) 610 MHz. The central core emission, the inner and outer cones are identified in each panel. The components show different spectral evolution, with the core emission having the steepest spectra, while the outer cone shows higher relative intensity at the lower frequency compared to the inner cones.

Table 3. Spectral Difference across the profile

	PSR	Type	$\Delta\alpha_{core-cone}$	$\Delta\alpha_{in-out}$	$\Delta\alpha_{core-in}$	$\Delta\alpha_{core-out}$
1	B0450–18	T	-0.998 ± 0.040	—	—	—
2	B0626+24	$T_{1/2}$	-0.681 ± 0.037	—	—	—
3	B0844–35	cQ	—	0.61 ± 0.14	—	—
4	B0919+06	T	-0.501 ± 0.044	—	—	—
5	J1034–3224	cQ	—	0.423 ± 0.066	—	—
6	B1237+25	M	-0.341 ± 0.022	0.138 ± 0.022	-0.435 ± 0.046	-0.297 ± 0.022
7	B1325–49	M	-0.279 ± 0.044	0.120 ± 0.044	-0.36 ± 0.14	-0.244 ± 0.044
8	B1700–32	T	-0.409 ± 0.040	—	—	—
9	B1732–07	T	-0.911 ± 0.040	—	—	—
10	B1737+13	M	-0.813 ± 0.051	0.568 ± 0.069	-1.169 ± 0.057	-0.601 ± 0.051
11	B1738–08	cQ	—	0.363 ± 0.095	—	—
12	B1745–12	cT/cQ	—	0.112 ± 0.033	—	—
13	B1758–29	T	-0.64 ± 0.18	—	—	—
14	B1821+05	T	-0.91 ± 0.12	—	—	—
15	B1831–04	M	-0.93 ± 0.14	0.42 ± 0.18	-1.23 ± 0.15	-0.82 ± 0.14
16	B1857–26	M	-1.043 ± 0.062	0.319 ± 0.073	-1.223 ± 0.062	-0.904 ± 0.062
17	B1907+10	$T_{1/2}$	-0.825 ± 0.040	—	—	—
18	B1914+09	$T_{1/2}$	-0.80 ± 0.24	—	—	—
19	B1917+00	T	-0.980 ± 0.062	—	—	—
20	B2045–16	T	-0.452 ± 0.011	—	—	—
21	B2327–20	T	-0.581 ± 0.018	—	—	—

difference in the spectral index between the different component types are unaffected. The difference in spectral index between the core and the conal components ($\Delta\alpha_{core-cone}$) can be obtained as :

$$\begin{aligned}\Delta\alpha_{core-cone} &= \log\left(\frac{S_{core}^{\nu_1}}{S_{core}^{\nu_2}}\right) / \log\left(\frac{\nu_1}{\nu_2}\right) - \log\left(\frac{S_{cone}^{\nu_1}}{S_{cone}^{\nu_2}}\right) / \log\left(\frac{\nu_1}{\nu_2}\right), \\ &= \log\left(\frac{S_{core}^{\nu_1}}{S_{cone}^{\nu_1}}\right) / \log\left(\frac{\nu_1}{\nu_2}\right) - \log\left(\frac{S_{core}^{\nu_2}}{S_{cone}^{\nu_2}}\right) / \log\left(\frac{\nu_1}{\nu_2}\right).\end{aligned}\quad (1)$$

Here S_{core}^{ν} and S_{cone}^{ν} gives estimates of the flux density of the core and conal component at a given frequency (ν), and $S_{core}^{\nu}/S_{cone}^{\nu}$ removes the effect of scintillation. The spectral index difference between the inner and outer conal components ($\Delta\alpha_{in-out}$), the core and inner cone ($\Delta\alpha_{core-in}$) and the core and outer cone ($\Delta\alpha_{core-out}$), can also be estimated in a similar manner.

$$\begin{aligned}\Delta\alpha_{in-out} &= \log\left(\frac{S_{in}^{\nu_1}}{S_{out}^{\nu_1}}\right) / \log\left(\frac{\nu_1}{\nu_2}\right) - \log\left(\frac{S_{in}^{\nu_2}}{S_{out}^{\nu_2}}\right) / \log\left(\frac{\nu_1}{\nu_2}\right), \\ \Delta\alpha_{core-in} &= \log\left(\frac{S_{core}^{\nu_1}}{S_{in}^{\nu_1}}\right) / \log\left(\frac{\nu_1}{\nu_2}\right) - \log\left(\frac{S_{core}^{\nu_2}}{S_{in}^{\nu_2}}\right) / \log\left(\frac{\nu_1}{\nu_2}\right), \\ \Delta\alpha_{core-out} &= \log\left(\frac{S_{core}^{\nu_1}}{S_{out}^{\nu_1}}\right) / \log\left(\frac{\nu_1}{\nu_2}\right) - \log\left(\frac{S_{core}^{\nu_2}}{S_{out}^{\nu_2}}\right) / \log\left(\frac{\nu_1}{\nu_2}\right).\end{aligned}\quad (2)$$

Here S_{in}^{ν} is the flux density of the inner conal components, S_{out}^{ν} for the outer conal components.

There were 21 pulsars in the MSPES list where we were able to separate the different component types within the same profile. Table 3 shows the estimates of the spectral index difference for these sources. The list included 17 pulsars with M, T and $T_{1/2}$ profiles and showed the core emission to have a much steeper spectra in all cases, with an average $\Delta\alpha_{core-cone} = -0.71$ between 325 and 610 MHz. In addition to the 5 pulsars with M type profiles with all three types of components, there were an additional 4 pulsars with ${}_cQ$ profiles where the inner and the outer conal components could be discerned. The outer conal components showed a steeper spectra compared to the inner cone with the average $\Delta\alpha_{in-out} = 0.34$. The difference of the spectral behaviour is also illustrated in the profiles shown in Fig. 3, where the core emission shows a much higher intensity at the lower frequency compared to both the inner and outer cones, while the outer cone is brighter at the lower frequency compared to the inner cone. In PSR B1237+25 there were two different emission modes with very different profile shapes (see below) and the spectral estimates were carried out only for the ‘normal’ mode.

5. EMISSION MODES

We have searched for the presence of mode changing in the single pulse emission of the MSPES sample by careful visual inspection of the single pulse sequence. The limitation of a survey setup, where the pulsars were observed for short durations of 2100 pulses, was not conducive for detecting longer duration mode changes with typical durations of hours timescales. We have identified 12 pulsars in our observations where the emission showed transition to different modes, 3 of these PSRs B0525+21, J1625–4048 and B1758–29, had no previous report of this phenomenon. In two other pulsars, B1819–22 and B2003–08, mode changing was first observed in the MSPES observations. More detailed studies have been carried out subsequently in these two sources to characterise the mode properties. We have measured the different mode behaviour including relative abundance, number of modes, average length, flux density and profile widths, that are reported in Table 4. In some cases the pulsar also showed the presence of nulling, lower intensity pulses or mixed states which could not be clearly classified within the individual modes. A short description of mode changing in each pulsar is presented below.

Table 4. Emission Mode Characteristics

PSR	Freq (MHz)	Npulse (P)	Mode	Avg. Flux (mJy)	Abundance (%)	Nmode	Avg. Length (P)	W_{10} ($^{\circ}$)	$W_{5\sigma}$ ($^{\circ}$)	
1	B0031–07	325	2099	A	116.4±4.4	12.2	6	51.0	40.3±0.3	42.8±0.3

Table 4 continued on next page

Table 4 (*continued*)

PSR	Freq (MHz)	Npulse (<i>P</i>)	Mode	Avg. Flux (mJy)	Abundance (%)	Nmode	Avg. Length (<i>P</i>)	W_{10} ($^{\circ}$)	$W_{5\sigma}$ ($^{\circ}$)	
			B	173.5 \pm 4.3	39.5	23	36.0	39.1 \pm 0.3	52.4 \pm 0.3	
			C	142.4 \pm 4.9	1.7	1	35.0	—	43.6 \pm 0.3	
2	B0525+21	325	424	A	189.9 \pm 5.0	51.2	5	43.4	19.9 \pm 0.3	23.5 \pm 0.3
				B	93.9 \pm 5.1	30.7	6	21.7	21.5 \pm 0.3	23.8 \pm 0.3
3	B0844-35	325	2149	A	14.1 \pm 1.6	90.8	12	162.7	33.7 \pm 0.5	34.2 \pm 0.5
				B	18.1 \pm 1.7	9.2	11	17.9	—	30.9 \pm 0.5
		610	2149	A	10.2 \pm 0.4	95.0	6	340.2	—	28.1 \pm 0.5
				B	12.2 \pm 0.8	5.0	5	21.6	—	18.1 \pm 0.5
4	B1237+25	325	4294	Normal	—	91.3	6	653.3	15.6 \pm 0.2	18.8 \pm 0.2
				Abnormal	—	8.7	4	93.3	16.6 \pm 0.2	18.2 \pm 0.2
		610	867	Normal	24.3 \pm 0.9	100	—	—	14.4 \pm 0.2	15.9 \pm 0.2
5	J1625-4048	610	1524	Bright	7.1 \pm 0.4	27.8	26	16.3	—	20.9 \pm 0.3
				Quiet	4.9 \pm 0.4	24.2	19	19.4	—	20.7 \pm 0.3
				Mixed	5.8 \pm 0.4	19.8	10	30.2	—	21.4 \pm 0.3
6	J1727-2739	610	2127	A	8.7 \pm 0.6	10.2	7	31.0	—	30.4 \pm 0.6
				B	10.8 \pm 0.4	12.4	17	15.5	—	32.2 \pm 0.6
7	B1758-29	325	2107	Bright	13.7 \pm 0.5	49.1	30	34.5	—	22.7 \pm 0.3
				Quiet	7.1 \pm 0.6	37.7	33	24.1	—	22.1 \pm 0.3
		610	2106	Bright	15.5 \pm 0.6	47.3	27	36.9	—	20.9 \pm 0.6
				Quiet	9.6 \pm 0.7	39.3	27	30.6	—	20.4 \pm 0.6
8	B1819-22	325	2112	A	20.4 \pm 0.5	52.0	12	91.6	22.7 \pm 0.8	27.6 \pm 0.8
				B	10.6 \pm 0.5	37.3	12	65.6	—	28.0 \pm 0.8
				Trans-A	14.6 \pm 0.7	5.5	6	19.3	—	23.7 \pm 0.8
		610	2189	A	20.2 \pm 0.7	49.4	14	77.3	15.1 \pm 0.8	17.8 \pm 0.8
				B	13.6 \pm 0.7	44.0	13	74.2	—	18.1 \pm 0.8
				Trans-A	20.9 \pm 1.2	2.6	3	18.7	—	15.9 \pm 0.8
9	B1839-04	610	1957	Bright	26.8 \pm 0.7	24.9	5	97.6	—	75.4 \pm 0.8
				Quiet	16.8 \pm 0.7	72.5	5	283.6	—	78.5 \pm 0.8
10	B1944+17	325	5569	A	145.9 \pm 2.3	7.1	8	49.5	34.1 \pm 0.8	49.8 \pm 0.8
				B	119.9 \pm 2.6	2.1	4	29.0	35.0 \pm 0.8	40.6 \pm 0.8
				C	114.2 \pm 2.3	11.1	69	8.0	32.5 \pm 0.8	45.0 \pm 0.8

Table 4 *continued on next page*

Table 4 (continued)

PSR	Freq (MHz)	Npulse (<i>P</i>)	Mode	Avg. Flux (mJy)	Abundance (%)	Nmode	Avg. Length (<i>P</i>)	W_{10} ($^{\circ}$)	$W_{5\sigma}$ ($^{\circ}$)	
			D	48.9±2.3	12.6	65	10.8	36.2±0.8	41.4±0.8	
	610	2179	A	168.2±2.4	12.6	7	39.1	36.6±0.8	42.6±0.8	
			B	151.0±4.3	1.0	1	21.0	—	28.5±0.8	
			C	158.9±2.3	13.8	36	13.8	32.9±0.8	43.0±0.8	
			D	71.6±2.4	9.9	19	11.4	—	37.0±0.8	
11	B2003-08	325	2134	A	66.1±2.3	6.8	3	48.7	—	70.1±0.9
			B	46.0±2.1	28.4	3	202.3	—	69.9±0.9	
			C	33.6±2.6	2.1	5	9.0	—	70.5±0.9	
			D	62.9±2.1	22.4	40	11.9	—	69.0±0.9	
	610	1491	A	43.3±1.6	18.9	2	141.0	—	58.9±0.9	
			B	27.9±1.6	20.2	2	150.5	—	58.5±0.9	
			C	16.3±1.8	7.4	9	12.3	—	62.8±0.9	
			D	43.6±1.7	10.0	17	8.8	—	61.9±0.9	
12	B2303+30	325	1699	Bright	30.4±0.9	54.4	23	40.2	8.4±0.6	11.8±0.6
			Quiet	15.7±1.0	34.7	27	21.8	10.4±0.6	12.1±0.6	

B0031-07 : The radio emission in this pulsar has been investigated in detail and shows the presence of three distinct drift modes A, B and C as well as nulling (Huguenin et al. 1970; Vivekanand & Joshi 1997; Smits et al. 2005; McSweeney et al. 2017). The 610 MHz observations were affected by RFI and could not be used for these studies. At 325 MHz we detected all three drift modes, with mode B being the most abundant, seen around 40 percent of the total duration, mode A was seen for around 12 percent of times, while mode C was seen only for a single sequence of 35 periods. The average profiles in each mode is shown in the appendix, Fig.7, which highlights the emission during mode A to be restricted near the trailing edge with a narrower width (see Table 4). The pulsar was around 50 percent brighter during mode B in comparison with mode A. Mode C seemed to have a double peaked structure, but there were too few pulses to form a clear idea. The drifting behaviour in the three modes were consistent with previous reports in the literature.

B0525+21 : The pulsar has relatively longer period (~ 3.7 seconds) and was observed for around 800 pulses at 325 MHz. The later half of the observations were affected by RFI and only 424 single pulses could be used for these studies. The pulsar has a classical double conal profile with two clearly separated components connected by a bridge emission and shows the presence of nulling. We have detected the presence of two distinct states in the single pulse emission, as shown in Fig.4a, which has not been reported earlier. Mode A consisted of bunches of bright emission in both the leading and trailing components. In contrast the emission during mode B was mostly seen as single bright pulses, primarily towards the trailing edge followed by low level emission or nulls. The average profiles corresponding to the two modes (see Fig.8 in appendix) show the leading component to be brighter in mode A with the bridge emission between the components also being more enhanced compared to mode B. The flux density as well as the average duration of mode A was twice as large compared to mode B. The pulsar was seen for around 50 percent of times in mode A and around 30 percent of the duration in mode B, but longer observations are required to develop better statistics of the modes.

B0844-35 : The pulsar has a four component conal profile of ${}_cQ$ type, with the third component being most prominent at both frequencies. The presence of mode changing was reported in Wang et al. (2007), with the central parts of the profile becoming bright during a short duration B mode. We have detected the presence of the

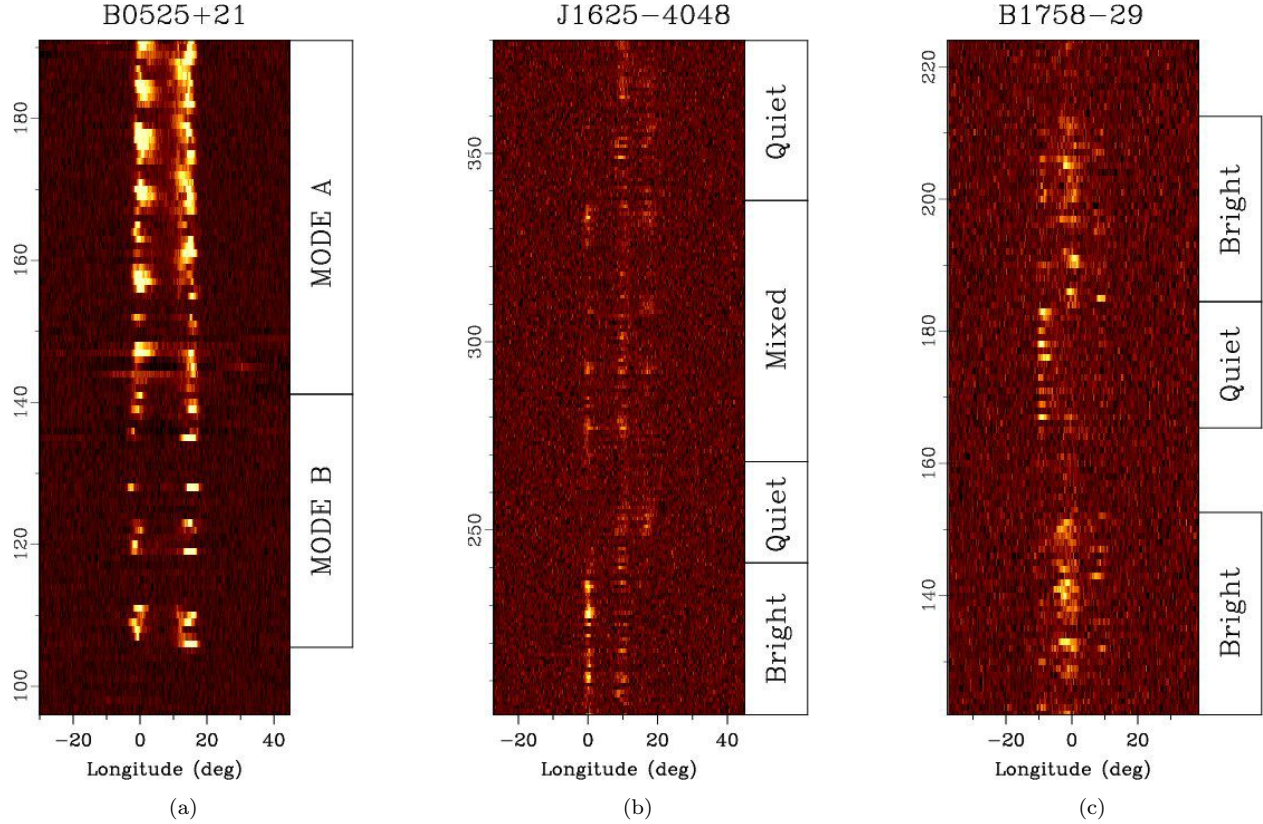


Figure 4. The figure shows the mode changing behaviour seen in the single pulse emission of the three pulsars where this phenomenon is reported for the first time. (a) The single pulses between pulse 95 and 190 from the start of the observation in PSR B0525+21 at 325 MHz. The transition from mode B to mode A is seen along with null pulses at the beginning as well as interspersed within the modes. (b) The transitions between the Bright, Weak and Mixed modes in PSR J1625-4048 at 610 MHz. The figure shows the single pulses between pulse 200 and 380 from the start of the observation. (c) The transitions between the Bright and Quiet modes in PSR B1758-29 at 325 MHz. The single pulses between 121 and 223 from the start of the observation are shown in the figure which also shows the presence of nulls.

centrally bright B mode for around 5-10 percent of times at both observing frequencies. Mode B was seen for short durations of around 20 periods while the much longer duration mode A was seen for hundreds of periods at a time. The second component was comparable to the much brighter third component in Mode B (see Fig.9 in appendix).

B1237+25 : The pulsar has a five component, M type, profile with well resolved core, inner and outer cones. The single pulse emission has been studied in detail and shows the presence of subpulse drifting, nulling and two modes, characterised as normal and abnormal (Backer 1970a,b; Srostlik & Rankin 2005; Smith et al. 2013; Maan & Deshpande 2014). The pulsar was observed on two separate occasions at 325 MHz, while at 610 MHz the observations lasted 867 pulses. The mode changing was seen at 325 MHz where the pulsar existed in the abnormal mode for around 9 percent of the total duration. Only the normal mode was seen during the shorter 610 MHz observations. The leading part of the profile, comprising of the first three components, became brighter during the abnormal mode while the trailing part was much weaker, compared to the normal mode (see Fig.10 in appendix).

J1625-4048 : The average profile shows the presence of three well separated components, with the central component identified as a core. The pulsar was only observed at 610 MHz and the single pulse emission showed the presence of three different modes, as shown in Fig.4b, that have not been reported earlier. The core emission remained roughly constant during the three modes, which showed variations in the leading and trailing components. In case of the bright mode the emission in the leading component was enhanced to around four times the central core level while the trailing component had very little intensity (see Fig.11 in appendix). In contrast during the quiet mode the leading

component was mostly missing but the trailing component was more prominent and comparable to the central core. In the third mixed mode all three components had similar intensities. All three modes were seen for similar durations, between 20-30% of the observing time (see Table 4), with the pulsar being in the null state for the remaining time.

J1727–2739 : The pulsar has a double conal profile with two well separated components. The single pulse emission has been studied in [Wen et al. \(2016\)](#) and showed the pulsar to exist mostly in the null state with relative abundance of around 70 percent. The radio emission during the burst state showed two distinct drift modes A and B, with periodicities of around $10P$ and $5P$ respectively, and a non-drifting mode C. The detection sensitivity at 325 MHz was insufficient for these studies and the modal behaviour was estimated at 610 MHz. We detected the two drifting modes A and B which were present for around 10 percent and 12 percent times, respectively. The third non-drifting mode C was not visible during these observations.

B1758–29 : We have detected the presence of mode changing in this pulsar with a three component T type profile and a central core. The pulsar showed the presence of a Bright and Quiet mode as shown in Fig.4c. The Bright mode had higher intensity in the core, while the core vanished in the Quiet mode. The average profiles of the two modes are shown in Fig.12. The pulsar was seen around 50 percent of time in the Bright mode and roughly 40 percent of time in the Quiet mode. The single pulse emission also showed the presence of nulls and low intensity level where the modal identification was not possible.

B1819–22 : The single pulse emission of this conal pulsar has been studied in [Basu & Mitra \(2018b\)](#), and showed the presence of three drifting modes and a non-drifting mode. The most abundant mode A had prominent drifting features, while it was absent during mode B. The short duration Trans-A was seen in some cases during transitions from mode A, and had a different drifting periodicity. A rare mode C with distinct behaviour was absent during the MSPES observations. The profiles of modes A, B and Trans-A at both observing frequencies are shown in Fig.14 in appendix, while the different modal characteristics are reported in Table 4.

B1839–04 : The pulsar has a double component conal profile with a prominent bridge emission between the two components. The presence of two emission modes, classified as the Bright and Quiet modes, was reported in this pulsar ([Weltevrede 2016](#)). The more abundant Q mode showed regular drifting behaviour, which was absent in the B mode. The 325 MHz observations were affected by scattering which made them unsuitable for identifying the emission modes. The modal analysis was carried out at 610 MHz and the characteristics of the two modes are reported in Table 4, while the average profiles are shown in Fig.13 in appendix.

B1944+17 : The single pulse emission of this conal pulsar showed the presence of three drifting modes A, B and C, and one non-drifting mode D ([Deich et al. 1986](#); [Kloumann & Rankin 2010](#)). The pulsar emission was dominated by nulling with more than 70 percent of time the single pulses were in the null state. The modes could be distinguished visually due to the different drift behaviour, with mode A having periodicity of around $14P$ and mode B around $6P$. Mode C seemed to have longer periodicity which could not be estimated due to the emission being frequently interrupted by nulls. The details of the mode behaviour at both observing frequencies are presented in Table 4. We have also estimated the average profiles in each mode which are shown in Fig.15 (see appendix).

B2003–08 : This five component pulsar with a M type profile showed the presence of four different modes as well as nulling in the single pulse emission ([Basu et al. 2019b](#)). The two modes A and B had subpulse drifting with different periodicities, with the core emission being more prominent in mode A. The core showed higher intensity during mode D which also had periodic nulling behaviour. In contrast the core was mostly absent during mode C which was also interspersed with nulls. The modal statistics during the MSPES observations at both frequencies are shown in Table 4 with the respective profile shapes in Fig.16 (see appendix).

B2303+30 : The pulsar showed the presence of a Bright and Quiet mode in the single pulse emission ([Redman et al. 2005](#)). Subpulse drifting was seen in each mode, with mode B having periodicity of around $2P$ and mode Q mode around $3P$. The pulsar was observed only at 325 MHz and we detected both the emission modes. The B mode had twice the intensity of the Q mode and was also present for longer durations. The characteristics of the two modes

are reported in Table 4 and the profiles are shown in Fig.17 in appendix.

In addition to the pulsars discussed above the presence of mode changing has also been reported in the pulsar B1918+19 (Hankins & Wolszczan 1987; Rankin et al. 2013), which was observed in MSPES, but the single pulses were detected with low sensitivity and the mode identification was not possible.

6. BURSTING EMISSION

We have observed several instances where the pulsar showed enhanced emission within the pulse window. There have been several reports of such behaviour in pulsars, the most prominent being the giant pulses which are short bursts of emission with energy greatly exceeding the average level (Lundgren et al. 1995; Kazantsev & Potapov 2018). In other cases ‘flaring’ has been found over a wider window in pulsars with asymmetric profile shapes (Mitra & Rankin 2011). Increased emission has also been reported at the onset of the mode changing in both the main pulse and postcursor components of PSR B0823+26 (Basu & Mitra 2019). Unlike mode changing these enhanced emission states are seen for short durations usually a single period and do not show any periodicity which distinguish them from periodic amplitude modulation (Basu et al. 2020). It is worth mentioning that Gil & Melikidze (2005) suggested a model for the enhanced emission based on the coherent curvature emission mechanism. They argued that the short observed time scale results from angular beaming due to the relativistic motion of localized sources along dipolar field lines, which involves a well-known “kinematic boosting” effect that shortens the apparent duration and consequently increases the apparent brightness of the observed signal.

In the description below we have categorised the pulsars into two groups, the first group consists of 7 pulsars where increased emission was seen mostly throughout the pulse window, and in the second group there are also 7 cases with the emission seen as flaring within a specific longitude range of the pulse window.

6.1. Short duration enhanced emission

B0540+23 : The pulsar profile has a single component with extended emission seen in the trailing edge. The radio emission was primarily in the form of bursts which were much narrower than the pulse window, but distributed throughout, as shown in Fig.5a. The peak flux level in the bursts reached more than 36 times the profile peak at 325 MHz and around a factor of 49 at 610 MHz. In 3-4 percent of pulses the peak flux were more than 10 times the average profile level.

B0611+22 : The bursting emission in this pulsar has been observed in the earlier studies of Seymour et al. (2014); Rajwade et al. (2016). The pulsar had a single component profile where the emission was seen throughout the pulse window. The burst state was seen primarily for short durations of few pulses as well as one relatively long stretch of around 50-60 pulses. The intensities of the bursting pulses were 5-10 times higher than the average value and were extended towards the trailing edge. The burst state was seen for around 15-20 percent of the observing duration at 325 MHz. The single pulses were detected with lower sensitivity at 610 MHz and the different states could not be distinguished.

B0656+14 : The presence of ‘spiky’ emission has been reported in this pulsar, where bursts were seen within a narrow longitude range of the pulse window (Weltevrede et al. 2006). We detected pulses with peak intensities which exceeded the average profile peak level by a factor of 50 in around 2 percent of pulses, with the maximum level being more than 240 times the average peak level at 325 MHz. At 610 MHz the maximum intensity level was more than 125 times the average profile peak and the intensities exceeded the average peak level by a factor of 40 around 2% of the observing duration.

B0727-18 : The pulsar showed bursts of emission in the single pulses as shown in Fig.5b, with maximum intensity exceeding more than 35 times the average peak. The pulsar has a double component profile connected by a prominent central bridge. The bursts were seen in both components as well as the connecting bridge region. In around 2 percent of pulses the intensity level within the pulse window exceeded 10 times the profile peak level.

B1742-30 : The pulsar profile show the presence of a leading component well separated from a double central structure which is followed by low level emission in the trailing side. The single pulses were seen primarily as short

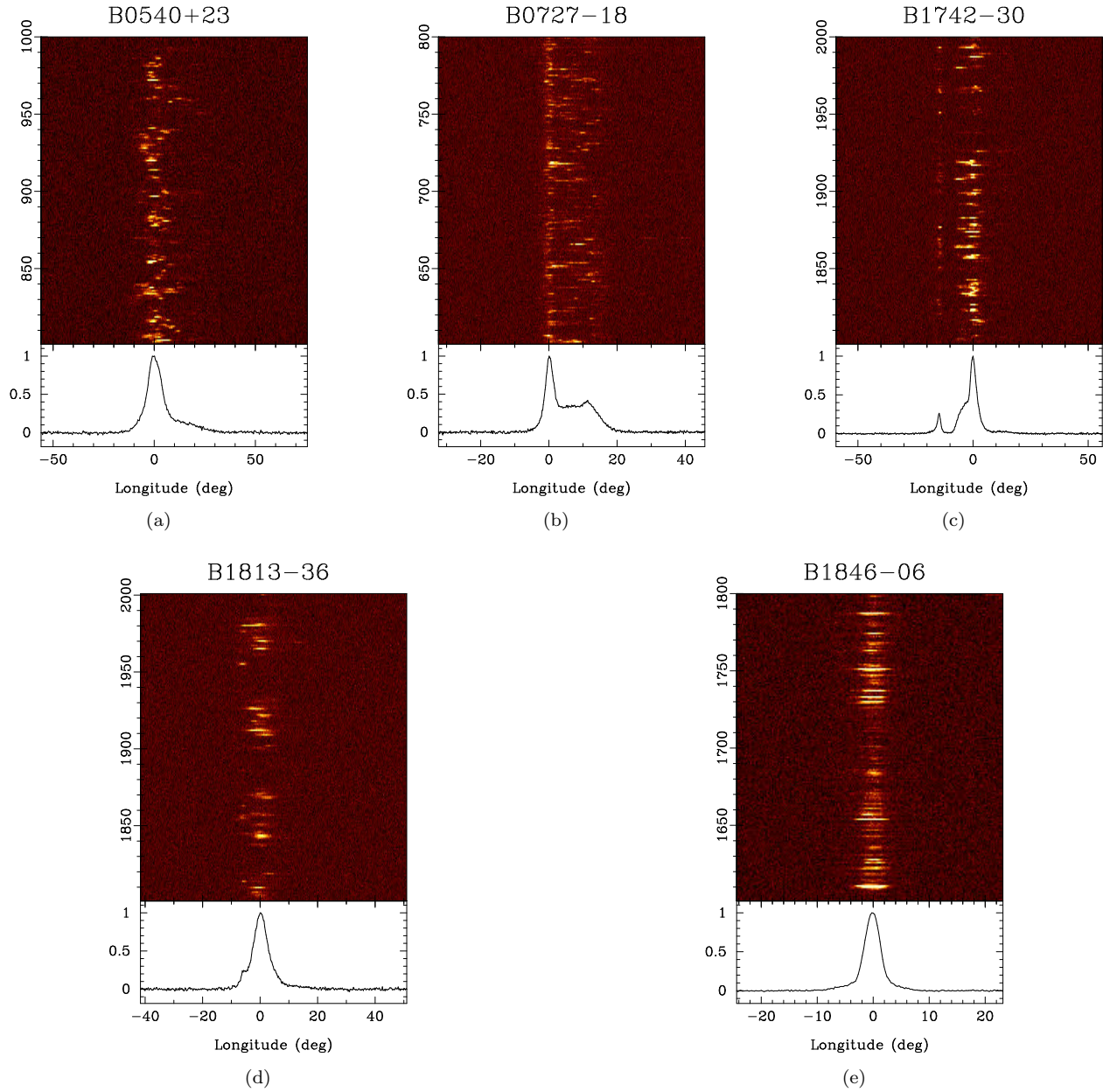


Figure 5. The figure shows the bursting emission in the single pulses (top panel) and the average profile (bottom panel). (a) PSR B0540+23 at 325 MHz. (b) B0727-18 at 325 MHz. (c) PSR B1742-30 at 610 MHz. (d) B1813-36 at 325 MHz. (e) B1846-06 at 610 MHz.

duration bursts as shown in Fig.5c. The maximum intensities in the single pulses were around a factor of 30 more than the average profile peak at both frequencies. In around 3 percent of the observing duration the peak pulse intensity was more than 10 times the peak flux density of the average profile.

B1813-36 : The pulsar show a single component profile with a narrow emission feature near the leading edge. The observations were carried out only at 325 MHz and Fig.5d shows a short section of the single pulses which were seen as short bursts across the pulse window. The maximum intensity in the single pulses was around a factor 24 higher than the profile peak, while strong bursts in excess of 5 times the average peak was seen in 7 percent of the total observed pulses.

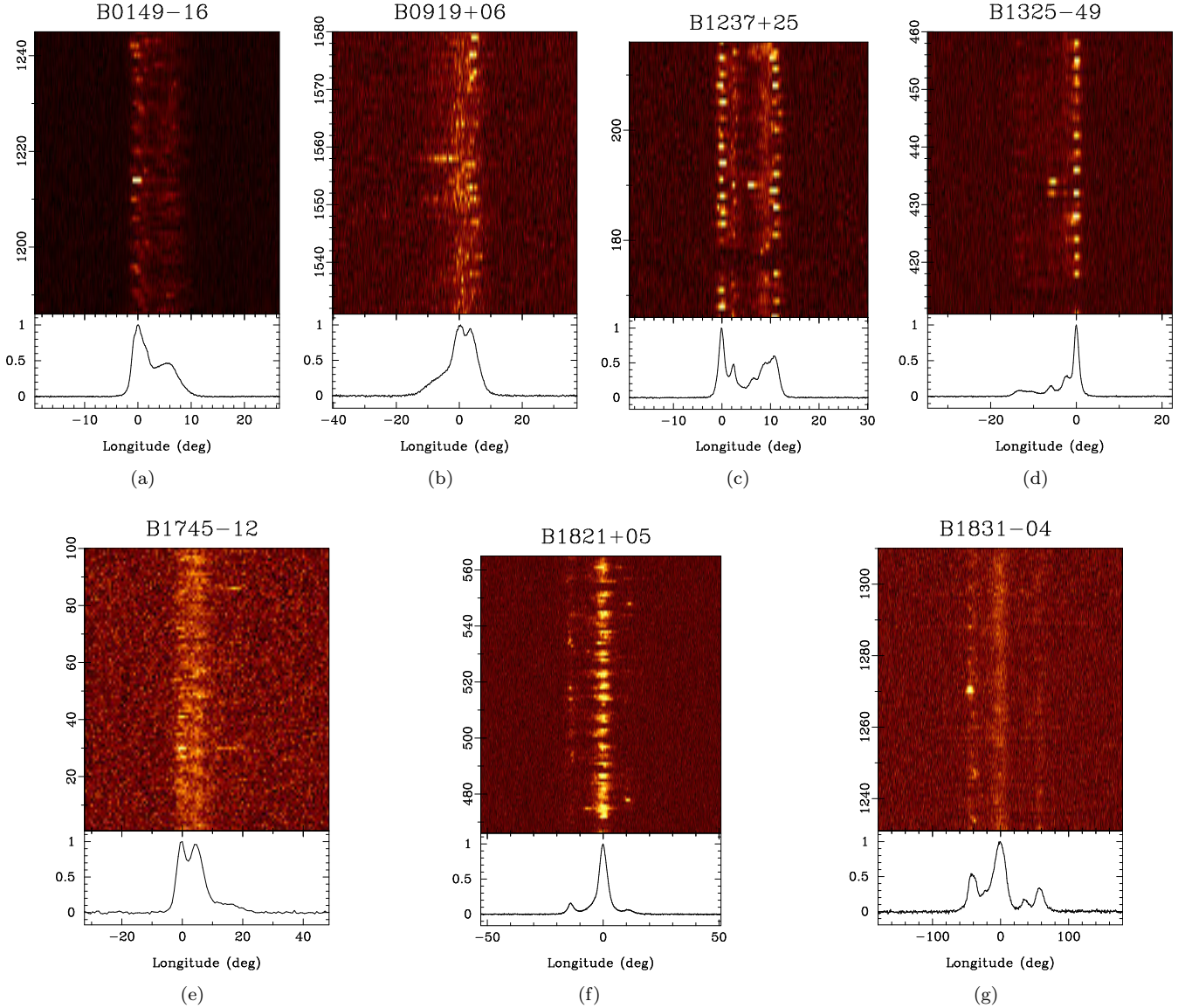


Figure 6. The figure shows examples of enhanced emission within a narrow range of the pulse window (top panel) along with the average profile (bottom panel). (a) Flaring in the leading component of PSR B0149-16. (b) Flaring in the leading edge of PSR B0919+06. (c) Bursts of emission in central component of PSR B1237+25. (d) Bursts of emission in central component of PSR B1325-49. (e) Flaring in trailing edge of PSR B1745-12. (f) Bursts of emission in trailing component of PSR B1821+05. (g) Flaring in leading component of PSR B1831-04.

B1846-06 : The pulsar has a single component profile at 610 MHz, while the lower frequency is affected by scattering resulting in an elongated trailing edge. Bursts of short durations across the entire profile window were seen in conjunction with the lower intensity pulses (see Fig.5e). The maximum intensity in the bright pulses reached a level of more than 22 times the average profile peak, and in 5 percent of single pulses the peak intensity was more than 5 times the average level.

6.2. Flaring within the pulse window

B0149-16 : The pulsar has a double component profile and show the presence of subpulse drifting. Narrow flaring events were seen in leading component as shown in Fig.6a, where the intensity was greatly increased to a maximum level of more than 30 times the average energy. Such events were however rare and seen in only around 0.8 percent of

the total pulses.

B0919+06 : The pulsar profile show low level extended emission in the leading edge which connects with a higher intensity double peaked structure in the trailing side. Flaring was seen in the leading part of the pulse window as shown in Fig.6b. However, they were rarely seen in the single pulses, with less than 10 events recorded during 2100 pulses observed. The intensities of the flares were a factor of 5-10 times more than the average intensity.

B1237+25 : The pulsar has a five component profile with a central core emission. There are two emission modes in this pulsar, as reported above, the normal mode where the core is weaker than the conal emission and an abnormal mode with the central region becoming brighter. In the normal mode there were instances when the core emission showed flaring in intensity, around 10-20 times the average level as shown in Fig.6c. These flaring events were rare and seen in less than 1 percent of the observed pulses.

B1325-49 : The pulsar has an asymmetric multi-component profile with the trailing side being much more prominent than the leading part. In rare cases the central component showed flaring which had intensities of around 10-20 times the mean level (see Fig.6d). These flares were seen in less than 10 pulses during the observing sessions.

B1745-12 : The pulsar has two distinct components in the leading edge followed by a wide low level emission in the trailing side. There were flaring events in the weak trailing side, as shown in Fig.6e, which were comparable to the leading emission and were a factor of 10-20 times greater than the average level. However, these were rare events seen in less than 1 percent of the total pulses.

B1821+05 : The pulsar has a triple component profile with a prominent central core component and weak leading and trailing cones. The emission in the trailing side was mostly seen as short duration bursts (see Fig.6f) with maximum intensity more than 30 times the average profile level. In around 5 percent of times the emission in the trailing component had peak intensity in excess of 10 times the average value.

B1831-04 : The pulsar has a multi-component profile with a prominent core and outer cones as well as clearly distinguishable inner conal components. The leading outer cone showed flaring events where the emission increased in intensity by a factor of 10-20 times the average level as shown in Fig.6g. However, these events were rare and seen in less than 20 pulses over the entire observing duration.

7. CONCLUSION

We have measured the flux density of 113 pulsars observed in the Meterwavelength Single-pulse Polarimetric Emission Survey, at 325 and 610 MHz, by making images from the interferometric observations of these sources. We have explored different emission features of these sources related to the variations in the average profile and single pulses. We have estimated the spectral variation across the emission beam in 21 pulsars with clearly identified core, and inner and outer conal components, where the steepest spectra was seen in the central core region, while the outer cones had steeper spectra compared to the inner cones. The radio emission is believed to originate in the relativistically outflowing plasma along the open magnetic field lines, where plasma instabilities result in charge bunching that gives rise to coherent curvature radiation along the field lines (Melikidze et al. 2000; Gil et al. 2004; Lakoba et al. 2018; Rahaman et al. 2020). The observed radio emission is an incoherent addition of a large number of charge bunches, where each charge bunch emits coherently. Thus the observer cannot distinguish an individual charge bunch, but sees an average effect of the incoherently added power of a large number of individual charge bunches. The spectra of an individual charge bunch emitting curvature radiation depends on the Lorentz factor, the amount of charge in the bunch, the size of the bunch and the radius of curvature of the magnetic field. If we assume that the size of the total charge and Lorentz factor of the charge bunch are similar, then the spectral difference between the core and conal emission can be explained by the change in radius of curvature. In this case the steep spectra of the core emission implies that the radius of curvature does not vary much in the region where the core emission originates. Intuitively this seems to be reasonable, as the core emission arises from regions close to magnetic axis where the radius of curvature of the magnetic field lines do not vary much. Thus although there is incoherent averaging of the spectra, the spectra

of all the charge bunches are similar and hence the resultant spectra closely resemble a single particle charge bunch spectra. The conal emission arises from regions away from the magnetic axis, where across the conal emission regions variation of the radius of curvature is expected. This may lead to incoherent addition of spectra with slightly different spectral shape. This averaging can result in shallower spectra of the conal emission compared to the core emission. Alternatively, it is possible that the Lorentz factors or charge bunch variations can explain the change in spectral index across the window, however such effects can only be revealed by rigorous numerical simulations which is beyond the scope of this work.

Mode changing was found in two pulsars, B1819–22 and B2003–08, from the MSPES observations and were separately studied in earlier works. We have investigated in detail the single pulse emission and found 12 pulsars (~ 10 percent of the sample) to have different emission modes, including the two mentioned above. In three of these pulsars, B0525+21, J1625–4048 and B1758–29, this phenomenon has not been reported earlier. The observations usually spanned roughly 2100 pulses and were sensitive to short duration mode changing. A different state change was also seen in 7 pulsars where the emission was seen as short duration bursts across the emission window. In another 7 pulsars flaring in intensity across a narrower longitude range of the pulsed region was also characterised. These processes constitute changes in the steady state radio emission mechanism. In most cases discussed here the location of the radio emission within the magnetosphere appears to remain unaltered as suggested by the profile boundaries in the different states (see appendix B). As a result these state changes are likely to be driven by local changes of the magnetic field configuration near the polar cap, where the outflowing plasma is generated, thereby affecting the plasma parameters (a possible mechanism is presented in Geppert et al. 2021).

ACKNOWLEDGMENTS

We thank the referee for the comments that improved the paper. We thank the staff of the GMRT who have made these observations possible. The GMRT is run by the National Centre for Radio Astrophysics of the Tata Institute of Fundamental Research. DM acknowledges the support of the Department of Atomic Energy, Government of India, under project no. 12-R&D-TFR-5.02-0700. DM acknowledges funding from the grant “Indo-French Centre for the Promotion of Advanced Research - CEFIPRA” grant IFC/F5904-B/2018. This work was supported by the grant 2020/37/B/ST9/02215 of the National Science Centre, Poland.

REFERENCES

- Backer, D. C. 1970a, *Nature*, 228, 1297, doi: [10.1038/2281297a0](https://doi.org/10.1038/2281297a0)
- . 1970b, *Nature*, 228, 752, doi: [10.1038/228752a0](https://doi.org/10.1038/228752a0)
- Backus, I., Mitra, D., & Rankin, J. M. 2010, *MNRAS*, 404, 30, doi: [10.1111/j.1365-2966.2009.16102.x](https://doi.org/10.1111/j.1365-2966.2009.16102.x)
- Basu, R., & Mitra, D. 2018a, *MNRAS*, 475, 5098, doi: [10.1093/mnras/sty178](https://doi.org/10.1093/mnras/sty178)
- . 2018b, *MNRAS*, 476, 1345, doi: [10.1093/mnras/sty297](https://doi.org/10.1093/mnras/sty297)
- . 2019, *MNRAS*, 487, 4536, doi: [10.1093/mnras/stz1590](https://doi.org/10.1093/mnras/stz1590)
- Basu, R., Mitra, D., & Melikidze, G. I. 2017, *ApJ*, 846, 109, doi: [10.3847/1538-4357/aa862d](https://doi.org/10.3847/1538-4357/aa862d)
- . 2020, *ApJ*, 889, 133, doi: [10.3847/1538-4357/ab63c9](https://doi.org/10.3847/1538-4357/ab63c9)
- Basu, R., Mitra, D., Melikidze, G. I., et al. 2016, *ApJ*, 833, 29, doi: [10.3847/1538-4357/833/1/29](https://doi.org/10.3847/1538-4357/833/1/29)
- Basu, R., Mitra, D., Melikidze, G. I., & Skrzypczak, A. 2019a, *MNRAS*, 482, 3757, doi: [10.1093/mnras/sty2846](https://doi.org/10.1093/mnras/sty2846)
- Basu, R., Paul, A., & Mitra, D. 2019b, *MNRAS*, 486, 5216, doi: [10.1093/mnras/stz1225](https://doi.org/10.1093/mnras/stz1225)
- Basu, R., RoĹzko, K., Kijak, J., & Lewandowski, W. 2018, *MNRAS*, 475, 1469, doi: [10.1093/mnras/stx3228](https://doi.org/10.1093/mnras/stx3228)
- Becker, W., Kawai, N., Brinkmann, W., & Mignani, R. 1999, *A&A*, 352, 532, <https://arxiv.org/abs/astro-ph/9910010>
- Becker, W., Kramer, M., Jessner, A., et al. 2006, *ApJ*, 645, 1421, doi: [10.1086/504458](https://doi.org/10.1086/504458)
- Chen, J. L., Wang, H. G., Wang, N., et al. 2011, *ApJ*, 741, 48, doi: [10.1088/0004-637X/741/1/48](https://doi.org/10.1088/0004-637X/741/1/48)
- Cordes, J. M., & Lazio, T. J. W. 2002, arXiv e-prints, astro. <https://arxiv.org/abs/astro-ph/0207156>
- Cordova, F. A., Hjellming, R. M., Mason, K. O., & Middleditch, J. 1989, *ApJ*, 345, 451, doi: [10.1086/167918](https://doi.org/10.1086/167918)
- Deich, W. T. S., Cordes, J. M., Hankins, T. H., & Rankin, J. M. 1986, *ApJ*, 300, 540, doi: [10.1086/163831](https://doi.org/10.1086/163831)
- Dembska, M., Basu, R., Kijak, J., & Lewandowski, W. 2015, *MNRAS*, 449, 1869, doi: [10.1093/mnras/stv333](https://doi.org/10.1093/mnras/stv333)
- Dyks, J., Rudak, B., & Demorest, P. 2010, *MNRAS*, 401, 1781, doi: [10.1111/j.1365-2966.2009.15679.x](https://doi.org/10.1111/j.1365-2966.2009.15679.x)
- Esamdin, A., Abdurixit, D., Manchester, R. N., & Niu, H. B. 2012, *ApJL*, 759, L3, doi: [10.1088/2041-8205/759/1/L3](https://doi.org/10.1088/2041-8205/759/1/L3)

- Esamdin, A., Lyne, A. G., Graham-Smith, F., et al. 2005, *MNRAS*, 356, 59, doi: [10.1111/j.1365-2966.2004.08444.x](https://doi.org/10.1111/j.1365-2966.2004.08444.x)
- Fowler, L. A., Morris, D., & Wright, G. A. E. 1981, *A&A*, 93, 54
- Frail, D. A., Jagannathan, P., Mooley, K. P., & Intema, H. T. 2016, *ApJ*, 829, 119, doi: [10.3847/0004-637X/829/2/119](https://doi.org/10.3847/0004-637X/829/2/119)
- Geppert, U., Basu, R., Mitra, D., Melikidze, G. I., & Szkudlarek, M. 2021, *MNRAS*, doi: [10.1093/mnras/stab1134](https://doi.org/10.1093/mnras/stab1134)
- Gil, J., Lyubarsky, Y., & Melikidze, G. I. 2004, *ApJ*, 600, 872, doi: [10.1086/379972](https://doi.org/10.1086/379972)
- Gil, J., & Melikidze, G. I. 2005, *A&A*, 432, L61, doi: [10.1051/0004-6361:200500021](https://doi.org/10.1051/0004-6361:200500021)
- Han, J., Han, J. L., Peng, L.-X., et al. 2016, *MNRAS*, 456, 3413, doi: [10.1093/mnras/stv2891](https://doi.org/10.1093/mnras/stv2891)
- Han, J. L., & Tian, W. W. 1999, *A&AS*, 136, 571, doi: [10.1051/aas:1999234](https://doi.org/10.1051/aas:1999234)
- Hankins, T. H., & Wolszczan, A. 1987, *ApJ*, 318, 410, doi: [10.1086/165377](https://doi.org/10.1086/165377)
- Hermesen, W., Hessels, J. W. T., Kuiper, L., et al. 2013, *Science*, 339, 436, doi: [10.1126/science.1230960](https://doi.org/10.1126/science.1230960)
- Hermesen, W., Kuiper, L., Hessels, J. W. T., et al. 2017, *MNRAS*, 466, 1688, doi: [10.1093/mnras/stw3135](https://doi.org/10.1093/mnras/stw3135)
- Hermesen, W., Kuiper, L., Basu, R., et al. 2018, *MNRAS*, 480, 3655, doi: [10.1093/mnras/sty2075](https://doi.org/10.1093/mnras/sty2075)
- Huguenin, G. R., Taylor, J. H., & Troland, T. H. 1970, *ApJ*, 162, 727, doi: [10.1086/150704](https://doi.org/10.1086/150704)
- Jankowski, F., van Straten, W., Keane, E. F., et al. 2018, *MNRAS*, 473, 4436, doi: [10.1093/mnras/stx2476](https://doi.org/10.1093/mnras/stx2476)
- Kaplan, D. L., Condon, J. J., Arzoumanian, Z., & Cordes, J. M. 1998, *ApJS*, 119, 75, doi: [10.1086/313153](https://doi.org/10.1086/313153)
- Karastergiou, A., & Johnston, S. 2007, *MNRAS*, 380, 1678, doi: [10.1111/j.1365-2966.2007.12237.x](https://doi.org/10.1111/j.1365-2966.2007.12237.x)
- Kazantsev, A. N., & Potapov, V. A. 2018, *Research in Astronomy and Astrophysics*, 18, 097, doi: [10.1088/1674-4527/18/8/97](https://doi.org/10.1088/1674-4527/18/8/97)
- Kloumann, I. M., & Rankin, J. M. 2010, *MNRAS*, 408, 40, doi: [10.1111/j.1365-2966.2010.17114.x](https://doi.org/10.1111/j.1365-2966.2010.17114.x)
- Kouwenhoven, M. L. A. 2000, *A&AS*, 145, 243, doi: [10.1051/aas:2000240](https://doi.org/10.1051/aas:2000240)
- Kramer, M. 1994, *A&AS*, 107, 527
- Lakoba, T., Mitra, D., & Melikidze, G. 2018, *MNRAS*, 480, 4526, doi: [10.1093/mnras/sty2152](https://doi.org/10.1093/mnras/sty2152)
- Latham, C., Mitra, D., & Rankin, J. 2012, *MNRAS*, 427, 180, doi: [10.1111/j.1365-2966.2012.21985.x](https://doi.org/10.1111/j.1365-2966.2012.21985.x)
- Lewandowski, W., Wolszczan, A., Feiler, G., Konacki, M., & Sołtysiński, T. 2004, *ApJ*, 600, 905, doi: [10.1086/379923](https://doi.org/10.1086/379923)
- Lorimer, D. R., Yates, J. A., Lyne, A. G., & Gould, D. M. 1995, *MNRAS*, 273, 411, doi: [10.1093/mnras/273.2.411](https://doi.org/10.1093/mnras/273.2.411)
- Lundgren, S. C., Cordes, J. M., Ulmer, M., et al. 1995, *ApJ*, 453, 433, doi: [10.1086/176404](https://doi.org/10.1086/176404)
- Lyne, A. G. 1971, *MNRAS*, 153, 27P, doi: [10.1093/mnras/153.1.27P](https://doi.org/10.1093/mnras/153.1.27P)
- Lyne, A. G., & Manchester, R. N. 1988, *MNRAS*, 234, 477, doi: [10.1093/mnras/234.3.477](https://doi.org/10.1093/mnras/234.3.477)
- Maan, Y., & Deshpande, A. A. 2014, *ApJ*, 792, 130, doi: [10.1088/0004-637X/792/2/130](https://doi.org/10.1088/0004-637X/792/2/130)
- Maron, O., Kijak, J., Kramer, M., & Wielebinski, R. 2000, *A&AS*, 147, 195, doi: [10.1051/aas:2000298](https://doi.org/10.1051/aas:2000298)
- McSweeney, S. J., Bhat, N. D. R., Tremblay, S. E., Deshpande, A. A., & Ord, S. M. 2017, *ApJ*, 836, 224, doi: [10.3847/1538-4357/aa5c35](https://doi.org/10.3847/1538-4357/aa5c35)
- Melikidze, G. I., Gil, J. A., & Pataraya, A. D. 2000, *ApJ*, 544, 1081, doi: [10.1086/317220](https://doi.org/10.1086/317220)
- Mitra, D., Basu, R., Maciesiak, K., et al. 2016, *ApJ*, 833, 28, doi: [10.3847/1538-4357/833/1/28](https://doi.org/10.3847/1538-4357/833/1/28)
- Mitra, D., & Deshpande, A. A. 1999, *A&A*, 346, 906, <https://arxiv.org/abs/astro-ph/9904336>
- Mitra, D., & Rankin, J. M. 2002, *ApJ*, 577, 322, doi: [10.1086/342136](https://doi.org/10.1086/342136)
- . 2011, *ApJ*, 727, 92, doi: [10.1088/0004-637X/727/2/92](https://doi.org/10.1088/0004-637X/727/2/92)
- Perley, R. A., & Butler, B. J. 2017, *ApJS*, 230, 7, doi: [10.3847/1538-4365/aa6df9](https://doi.org/10.3847/1538-4365/aa6df9)
- Rahaman, S. k. M., Basu, R., Mitra, D., & Melikidze, G. I. 2021, *MNRAS*, 500, 4139, doi: [10.1093/mnras/staa3518](https://doi.org/10.1093/mnras/staa3518)
- Rahaman, S. M., Mitra, D., & Melikidze, G. I. 2020, *MNRAS*, 497, 3953, doi: [10.1093/mnras/staa2280](https://doi.org/10.1093/mnras/staa2280)
- Rajwade, K., Seymour, A., Lorimer, D. R., et al. 2016, *MNRAS*, 462, 2518, doi: [10.1093/mnras/stw1858](https://doi.org/10.1093/mnras/stw1858)
- Rankin, J. M. 1983, *ApJ*, 274, 333, doi: [10.1086/161450](https://doi.org/10.1086/161450)
- . 1990, *ApJ*, 352, 247, doi: [10.1086/168530](https://doi.org/10.1086/168530)
- . 1993, *ApJ*, 405, 285, doi: [10.1086/172361](https://doi.org/10.1086/172361)
- Rankin, J. M., Olszanski, T. E. E., & Wright, G. A. E. 2020, *ApJ*, 890, 151, doi: [10.3847/1538-4357/ab67cb](https://doi.org/10.3847/1538-4357/ab67cb)
- Rankin, J. M., Rodriguez, C., & Wright, G. A. E. 2006, *MNRAS*, 370, 673, doi: [10.1111/j.1365-2966.2006.10512.x](https://doi.org/10.1111/j.1365-2966.2006.10512.x)
- Rankin, J. M., Wright, G. A. E., & Brown, A. M. 2013, *MNRAS*, 433, 445, doi: [10.1093/mnras/stt739](https://doi.org/10.1093/mnras/stt739)
- Redman, S. L., Wright, G. A. E., & Rankin, J. M. 2005, *MNRAS*, 357, 859, doi: [10.1111/j.1365-2966.2005.08672.x](https://doi.org/10.1111/j.1365-2966.2005.08672.x)
- Rickett, B. J. 1990, *ARA&A*, 28, 561, doi: [10.1146/annurev.aa.28.090190.003021](https://doi.org/10.1146/annurev.aa.28.090190.003021)
- Seymour, A. D., Lorimer, D. R., & Ridley, J. P. 2014, *MNRAS*, 439, 3951, doi: [10.1093/mnras/stu250](https://doi.org/10.1093/mnras/stu250)
- Sieber, W. 1982, *A&A*, 113, 311
- Skrzypczak, A., Basu, R., Mitra, D., et al. 2018, *ApJ*, 854, 162, doi: [10.3847/1538-4357/aaa758](https://doi.org/10.3847/1538-4357/aaa758)
- Smith, E., Rankin, J., & Mitra, D. 2013, *MNRAS*, 435, 1984, doi: [10.1093/mnras/stt1404](https://doi.org/10.1093/mnras/stt1404)

- Smits, J. M., Mitra, D., & Kuijpers, J. 2005, *A&A*, 440, 683, doi: [10.1051/0004-6361:20041626](https://doi.org/10.1051/0004-6361:20041626)
- Sobey, C., Young, N. J., Hessels, J. W. T., et al. 2015, *MNRAS*, 451, 2493, doi: [10.1093/mnras/stv1066](https://doi.org/10.1093/mnras/stv1066)
- Srostlik, Z., & Rankin, J. M. 2005, *MNRAS*, 362, 1121, doi: [10.1111/j.1365-2966.2005.09390.x](https://doi.org/10.1111/j.1365-2966.2005.09390.x)
- Vivekanand, M., & Joshi, B. C. 1997, *ApJ*, 477, 431, doi: [10.1086/303690](https://doi.org/10.1086/303690)
- Wahl, H. M., Orfeo, D. J., Rankin, J. M., & Weisberg, J. M. 2016, *MNRAS*, 461, 3740, doi: [10.1093/mnras/stw1589](https://doi.org/10.1093/mnras/stw1589)
- Wang, H. G., Pi, F. P., Zheng, X. P., et al. 2014, *ApJ*, 789, 73, doi: [10.1088/0004-637X/789/1/73](https://doi.org/10.1088/0004-637X/789/1/73)
- Wang, N., Manchester, R. N., & Johnston, S. 2007, *MNRAS*, 377, 1383, doi: [10.1111/j.1365-2966.2007.11703.x](https://doi.org/10.1111/j.1365-2966.2007.11703.x)
- Wang, Q. D., Li, Z.-Y., & Begelman, M. C. 1993, *Nature*, 364, 127, doi: [10.1038/364127a0](https://doi.org/10.1038/364127a0)
- Weltevrede, P. 2016, *A&A*, 590, A109, doi: [10.1051/0004-6361/201527950](https://doi.org/10.1051/0004-6361/201527950)
- Weltevrede, P., Wright, G. A. E., Stappers, B. W., & Rankin, J. M. 2006, *A&A*, 458, 269, doi: [10.1051/0004-6361:20065572](https://doi.org/10.1051/0004-6361:20065572)
- Wen, Z. G., Wang, N., Yuan, J. P., et al. 2016, *A&A*, 592, A127, doi: [10.1051/0004-6361/201628214](https://doi.org/10.1051/0004-6361/201628214)
- Wright, G. A. E., & Fowler, L. A. 1981, *A&A*, 101, 356

Table 2. Flux Density measurement

	PSR	Date	325 MHz			Date	610 MHz		
			Avg Flux (mJy)	rms (mJy)	Peak Flux (mJy)		Avg Flux (mJy)	rms (mJy)	Peak Flux (mJy)
1	B0031-07	16/02/2014	92.7±4.3	2.0	1400±66	09/02/2014	22.4±4.2	1.2	—
2	J0134-2937	16/02/2014	8.1±1.3	0.7	225±36	09/02/2014	11.0±1.1	0.5	291±32
3	B0148-06	16/02/2014	8.4±2.8	1.4	184±61	23/03/2014	17.0±1.4	0.9	486±41
		09/03/2014	11.0±3.1	1.7	—				
4	B0149-16	16/02/2014	37.4±1.5	0.6	2406±98	09/02/2014	5.5±0.4	0.2	311±24
5	B0203-40	28/06/2014	37.8±3.2	1.6	3090±264	23/03/2014	1.1±0.5	0.3	112±48
6	B0301+19	27/03/2014	59.2±3.8	2.2	—	23/03/2014	28.3±0.9	0.2	1084±35
		28/06/2014	35.2±1.6	0.6	1395±63				
7	B0450-18	16/02/2014	124.9±5.0	1.5	2841±113	09/02/2014	74.6±2.1	0.4	1697±50
8	B0523+11	16/02/2014	22.4±2.1	1.1	866±83	09/02/2014	8.8±0.7	0.3	293±24
9	B0525+21	16/02/2014	88.5±5.0	1.8	3811±216				
10	B0540+23	16/02/2014	29.0±2.0	0.9	998±68	09/02/2014	37.0±1.3	0.4	1318±46
11	B0611+22	16/02/2014	23.3±2.3	1.1	1036±106	09/02/2014	15.7±0.8	0.4	855±56
12	B0626+24	16/02/2014	70.1±3.1	1.1	3410±149	09/02/2014	40.0±1.2	0.2	1805±54
13	B0628-28					23/03/2014	97.0±2.8	0.7	1657±48
14	B0656+14	16/02/2014	8.0±1.6	0.8	148±33	09/02/2014	8.0±0.5	0.2	180±15
		09/03/2014	4.0±0.6	0.4	—				
		28/06/2014	10.6±0.8	0.5	226±21				
15	B0727-18	28/06/2014	29.0±2.3	1.2	1298±104	23/03/2014	9.0±0.6	0.3	412±28
16	B0736-40	28/06/2014	318.5±9.2	1.7	1116±36				
17	B0740-28	09/03/2014	482.2±16.8	6.0	13955±487	23/03/2014	104.3±3.4	1.4	4469±147
18	B0756-15					23/03/2014	7.4±0.4	0.2	718±37
19	B0818-41					10/02/2014	22.7±0.7	0.2	121±8
20	B0834+06	14/02/2014	135.1±4.4	1.6	10446±341	10/02/2014	40.5±1.2	0.4	2925±90
21	B0844-35	09/03/2014	21.7±3.3	1.7	—	10/02/2014	10.3±0.4	0.1	396±17
		28/06/2014	15.6±1.6	1.0	391±41				
22	J0905-5127	28/06/2014	5.9±1.3	0.7	202±46				
23	B0919+06	28/06/2014	48.8±1.7	0.6	1690±61	20/03/2014	30.9±0.9	0.2	1490±45
24	B0942-13	28/06/2014	25.4±4.0	2.2	2416±379				
25	B0950+08	14/02/2014	981±29	6.9	21037±613	05/03/2014	88.8±2.5	0.4	1919±55
		16/02/2014	3813±105	11.9	63850±1754	07/03/2014	689±18	1.3	15693±429
		09/03/2014	603±19	3.1	16319±494	20/03/2014	232.2±6.4	0.7	5194±144
		19/03/2014	3019±84	11.7	60214±1691	23/03/2014	360±10	1.2	8407±232
		30/03/2014	2592±72	11.2	52113±1450				
		28/06/2014	71.9±3.6	1.7	1562±78				
		28/06/2014	370±11	2.6	8216±250				
26	J1034-3224	14/02/2014	45.1±1.2	1.0	831±24	10/02/2014	43.2±1.2	0.2	511±15

Table 2 continued on next page

Table 2 (continued)

PSR	Date	325 MHz			610 MHz				
		Avg Flux (mJy)	rms (mJy)	Peak Flux (mJy)	Date	Avg Flux (mJy)	rms (mJy)	Peak Flux (mJy)	
27	B1114-41				10/02/2014	9.9±0.6	0.4	717±43	
28	B1133+16	16/02/2014	334.2±10.8	2.9	24469±802	10/02/2014	66.1±2.1	0.6	5780±183
29	B1237+25				26/02/2014	24.3±0.9	0.5	1591±62	
30	B1254-10				05/03/2014	3.8±0.3	0.2	310±23	
31	B1325-49	16/02/2014	11.5±1.8	0.7	1387±216	05/03/2014	5.9±0.3	0.1	622±31
32	B1504-43	14/02/2014	8.9±2.5	1.3	509±142	05/03/2014	4.4±1.2	0.6	264±74
33	B1524-39				26/02/2014	4.3±0.3	0.2	390±27	
					26/02/2014	5.5±0.4	0.3	—	
34	J1549-4848	14/02/2014	8.8±1.0	0.6	310±35	26/02/2014	3.8±0.7	0.7	114±23
35	B1552-31	16/02/2014	18.8±1.0	0.5	644±37	26/02/2014	19.9±0.8	0.5	620±27
36	J1557-4258	02/03/2014	10.3±3.1	3.1	217±67	05/03/2014	13.4±2.4	1.3	836±152
37	B1556-44	14/02/2014	51.8±1.6	0.5	1767±56				
38	B1558-50	16/02/2014	12.1±1.1	0.6	244±23				
39	J1603-2531	28/03/2014	6.9±1.9	1.2	624±186	27/03/2014	8.9±0.5	0.3	463±29
40	B1600-49				23/03/2014	23.3±5.2	2.9	1410±313	
41	J1625-4048				07/03/2014	5.2±0.3	0.3	348±23	
42	B1642-03				07/03/2014	291.2±8.1	2.2	25953±721	
43	J1648-3256	30/03/2014	< 6.8	1.4	—	20/03/2014	3.1±0.7	0.5	201±47
44	J1700-3312	19/03/2014	< 3.6	0.8	—	20/03/2014	5.4±0.5	0.5	308±31
45	B1700-32	02/03/2014	30.8±1.3	0.6	904±38	07/03/2014	29.7±0.9	0.2	984±28
46	J1705-3423	02/03/2014	13.9±0.8	0.4	75±8	07/03/2014	15.0±0.5	0.3	279±13
		19/03/2014	24.0±1.1	0.5	129±15				
47	B1706-16	16/02/2014	66.7±0.9	0.4	3607±110				
48	B1706-44	14/02/2014	9.6±1.1	0.6	99±18	20/03/2014	13.2±0.7	0.4	171±12
		19/03/2014	14.0±1.6	0.9	137±24				
49	B1717-29				07/03/2014	43.6±1.5	0.6	1075±43	
50	B1718-32				10/02/2014	18.9±0.7	0.2	724±28	
51	B1719-37	14/02/2014	11.3±1.3	0.7	327±40	10/02/2014	7.3±1.3	0.8	311±54
52	J1727-2739				07/03/2014	2.2±0.2	0.1	56±7	
53	B1727-47	14/02/2014	76.2±2.2	0.4	4551±131	20/03/2014	65.4±1.8	0.1	5100±140
54	B1730-22	31/05/2014	24.9±1.2	0.6	902±43	07/03/2014	35.4±2.6	2.0	904±69
55	B1730-37	02/03/2014	2.5±0.5	0.4	—	20/03/2014	4.9±0.5	0.3	167±24
56	B1732-07	16/02/2014	55.8±1.6	0.7	3839±106				
57	B1736-29				07/03/2014	6.4±0.3	0.2	170±12	
58	B1737+13	12/07/2014	31.2±1.1	0.4	1419±50	26/02/2014	36.6±1.0	0.2	1265±37
59	B1737-39	19/03/2014	34.7±1.3	1.0	600±27	05/03/2014	21.2±0.7	0.2	1016±34
60	B1738-08	12/07/2014	10.7±0.4	0.2	354±16	23/03/2014	10.4±0.3	0.1	371±13
61	B1742-30	31/05/2014	9.4±0.6	0.3	276±18	10/02/2014	32.7±1.1	0.3	1804±59
62	B1745-12	16/02/2014	17.4±0.7	0.3	635±28				

Table 2 continued on next page

Table 2 (continued)

PSR	Date	325 MHz			610 MHz				
		Avg Flux (mJy)	rms (mJy)	Peak Flux (mJy)	Date	Avg Flux (mJy)	rms (mJy)	Peak Flux (mJy)	
63	J1750-3503	30/03/2014	10.4±0.9	0.5	120±17	27/03/2014	6.3±0.6	0.4	99±16
64	B1747-46	19/03/2014	68.9±2.2	0.7	3541±111	20/03/2014	34.3±1.0	0.2	2116±62
65	B1749-28	30/03/2014	238.1±6.5	0.6	17407±478	27/03/2014	311.5±8.7	2.2	27207±760
66	B1754-24	30/03/2014	4.6±1.1	0.7	—	27/03/2014	6.8±0.8	0.6	149±22
		27/07/2014	6.1±0.9	0.4	—				
67	B1758-03	28/03/2014	12.6±0.8	0.4	828±55	23/03/2014	5.4±0.3	0.1	470±26
68	B1758-29	30/03/2014	10.3±0.5	0.2	346±18	27/03/2014	10.5±0.3	0.2	388±19
69	B1804-08	28/03/2014	27.3±1.8	0.9	480±33	23/03/2014	40.4±1.6	0.7	1504±59
70	J1808-0813	28/03/2014	8.8±1.4	0.7	183±31	23/03/2014	8.7±0.6	0.3	307±23
71	B1813-26	30/03/2014	12.0±0.8	0.4	194±16	27/03/2014	7.4±0.8	0.4	186±24
72	B1813-36	19/03/2014	16.2±0.9	0.7	755±42				
73	J1817-3837	30/03/2014	4.8±2.1	0.9	223±97	27/03/2014	3.4±0.6	0.4	231±40
74	B1818-04	28/03/2014	148.8±4.9	1.3	6245±205	27/03/2014	62.1±2.2	0.8	4069±142
75	B1819-22	31/05/2014	16.2±0.5	0.1	402±13	27/03/2014	17.2±0.6	0.2	585±23
						27/03/2014	16.3±0.6	0.3	588±24
76	J1823-0154	28/03/2014	4.0±1.1	0.6	201±58	27/03/2014	3.2±0.4	0.3	383±53
77	B1821+05	02/03/2014	25.0±1.2	0.5	1504±73	26/02/2014	8.4±0.6	0.3	309±25
		12/07/2014	43.7±2.0	0.6	2512±118				
78	B1820-31	19/03/2014	45.5±1.6	0.6	2143±77	23/03/2014	17.3±0.8	0.4	897±45
		28/03/2014	46.7±2.1	0.9	2229±100				
79	B1831-04	19/03/2014	60.9±2.5	1.1	518±23	20/03/2014	53.7±1.8	0.7	334±13
80	J1835-1020	12/07/2014	3.1±1.3	0.7	—	07/03/2014	2.8±0.6	0.3	131±27
81	J1835-1106	12/07/2014	10.1±1.4	0.7	112±17	07/03/2014	5.2±0.7	0.5	175±27
82	B1839+09	02/03/2014	13.6±3.9	1.7	761±213	26/02/2014	9.8±0.7	0.4	498±37
83	B1839-04	19/03/2014	10.2±1.3	0.6	—	20/03/2014	17.9±0.7	0.3	235±13
		27/07/2014	11.4±0.7	0.3	72±8				
84	J1843-0000	19/03/2014	7.0±0.4	0.3	—	20/03/2014	8.1±0.3	0.1	191±9
		27/07/2014	7.7±0.5	0.2	—				
85	B1842+14	02/03/2014	36.0±1.1	0.3	1562±51	07/03/2014	7.5±0.3	0.2	313±16
		30/03/2014	26.3±2.2	1.4	1188±107				
86	B1844-04	19/03/2014	42.2±1.6	0.6	525±22	20/03/2014	15.6±0.5	0.2	586±22
87	B1845-01	21/06/2014	32.1±1.5	0.7	161±14	20/03/2014	26.8±1.3	0.7	657±34
88	J1848-1414	02/03/2014	< 4.1	0.8	—	07/03/2014	2.0±0.7	0.5	60±23
		27/07/2014	< 5.2	1.0	—				
89	B1846-06	31/05/2014	20.2±0.6	0.2	736±25				
		21/06/2014	16.6±0.5	0.2	615±21				
90	J1852-2610	21/06/2014	18.8±2.1	1.1	619±70				
91	B1857-26	12/07/2014	119.9±3.6	0.8	3397±103	09/02/2014	77.5±2.2	0.3	1236±38
92	J1901-0906	27/07/2014	7.8±0.4	0.2	818±47	07/03/2014	5.7±0.3	0.2	526±28

Table 2 continued on next page

Table 2 (continued)

PSR	Date	325 MHz			610 MHz				
		Avg Flux (mJy)	rms (mJy)	Peak Flux (mJy)	Date	Avg Flux (mJy)	rms (mJy)	Peak Flux (mJy)	
93	B1907+10	02/03/2014	36.3±1.4	0.6	1699±66	26/02/2014	14.0±1.6	0.9	937±108
94	B1907+03	12/07/2014	28.8±1.1	0.4	343±15	05/03/2014	15.7±0.5	0.1	227±10
95	B1911-04	14/02/2014	81.5±2.3	0.4	8863±252	10/02/2014	78.2±2.1	0.2	8005±220
96	B1914+09	02/03/2014	8.4±0.8	0.5	381±39	26/02/2014	6.2±1.2	0.7	268±54
		21/06/2014	10.6±1.3	0.5	488±59				
97	B1915+13	02/03/2014	35.9±1.1	0.3	1536±51	26/02/2014	10.2±0.9	0.5	566±49
		09/03/2014	41.5±1.6	0.5	1794±68				
98	B1917+00	02/03/2014	9.3±0.9	0.5	887±82	05/03/2014	4.6±0.4	0.2	389±35
		21/06/2014	18.7±1.1	0.5	1637±99				
99	J1919+0134	09/03/2014	2.4±0.5	0.4	—				
100	B1918+19	02/03/2014	19.8±1.0	0.5	326±18	26/02/2014	10.2±0.5	0.2	161±11
101	B1919+21					27/03/2014	31.1±0.9	0.3	1547±48
102	B1929+10	14/02/2014	127.8±3.9	1.0	4620±142	09/02/2014	137.2±4.4	1.6	4556±151
		16/02/2014	195.0±6.5	2.2	6555±218	10/02/2014	130.5±3.7	0.8	4828±139
		16/02/2014	390.9±11.4	2.6	13769±400	26/02/2014	34.6±1.2	0.5	1225±44
		02/03/2014	312.3±9.1	2.7	10956±320	26/02/2014	22.2±1.3	0.7	—
		09/03/2014	173.7±5.6	1.7	6763±217	05/03/2014	139.9±4.1	0.8	5401±155
		19/03/2014	139.9±4.6	1.7	5137±170	05/03/2014	244.1±7.4	2.3	—
		30/03/2014	344.6±14.6	7.7	12742±540	07/03/2014	123.2±3.4	0.5	4718±132
		31/05/2014	111.2±3.8	1.6	4040±137	07/03/2014	53.5±1.9	0.9	—
		21/06/2014	353.3±10.4	2.5	12467±368	20/03/2014	231.4±6.4	0.9	—
		12/07/2014	200.2±6.2	1.7	7036±217	20/03/2014	261.8±1.2	0.8	10021±276
	27/07/2014	243.5±8.0	3.2	8851±293	23/03/2014	129.9±3.8	1.0	4349±129	
	27/07/2014	73.1±2.6	1.0	2954±104	23/03/2014	81.2±2.5	0.8	5496±178	
					27/03/2014	58.5±1.8	0.8	2025±63	
103	B1937-26	16/02/2014	7.7±1.9	0.9	523±128				
104	B1944+17	16/02/2014	15.1±1.8	0.9	391±47	27/03/2014	51.6±1.6	0.5	996±34
		12/07/2014	34.8±2.2	1.2	728±46				
		27/07/2014	30.3±1.6	0.7	594±31				
105	B2003-08	14/02/2014	34.3±2.0	1.0	426±27	10/02/2014	18.5±1.5	0.8	247±24
106	B2043-04	14/02/2014	27.8±1.8	1.1	2278±147	10/02/2014	13.8±0.5	0.2	989±33
		16/02/2014	40.5±4.7	0.5	2878±335				
107	B2045-16	19/03/2014	221.5±6.3	1.3	10180±291	20/03/2014	75.4±2.3	0.9	4166±129
108	J2144-3933	16/02/2014	21.6±1.2	0.6	8472±476	09/02/2014	3.6±0.4	0.2	1700±177
109	B2303+30	27/07/2014	23.0±0.9	0.3	1648±65				
110	B2310+42	27/07/2014	90.8±3.4	1.5	4070±152				
111	B2315+21	09/03/2014	37.2±1.4	0.4	2469±93	27/03/2014	4.2±0.2	0.1	309±17
		21/06/2014	21.2±1.9	0.8	1635±148				
112	B2327-20				23/03/2014	12.6±0.4	0.1	1515±48	

Table 2 continued on next page

Table 2 (*continued*)

PSR	Date	325 MHz			610 MHz			
		Avg Flux (mJy)	rms (mJy)	Peak Flux (mJy)	Date	Avg Flux (mJy)	rms (mJy)	Peak Flux (mJy)
113 J2346-0609	09/03/2014	4.8±1.1	0.6	—	23/03/2014	4.8±0.3	0.2	264±18
	21/06/2014	10.3±1.6	0.8	399±61				

APPENDIX

A. ESTIMATING THE FLUX SCALE FROM CALIBRATORS

Table 5. Calibrator Sources

Date	Flux Cal	Flux (Jy)	Phase Cal	Flux (Jy)	Calibrated PSR
<u>325 MHz Observations</u>					
14/02/2014	3C286	26.4	2047-026	5.9	B2003-08, B2043-04
			1822-096	3.7	B1911-04, B1929+10
			1830-360	20.7	B1706-44, B1719-37, B1727-47
			1625-311	3.5	B1504-43, J1549-4848, B1556-44
			1021+219	6.6	B0950+08
			1033-343	4.8	J1034-3224
			0804+102	5.6	B0834+06
16/02/2014	3C48	43.9	0521+166	15.6	B0523+11, B0525+21, B0540+23, B0611+22, B0626+24, B0656+14
			0521-207	8.9	B0450-18
			0116-208	10.8	B0031-07, J0134-2937, B0148-06, B0149-16
	3C286	26.4	1830-360	21.5	B1937-26
			2047-026	6.2	B1929+10, B2043-04
			1924+334	6.2	B1929+10, B1944+17
			1625-311	3.2	B1552-31, B1558-50
			1822-096	3.6	B1706-16, B1732-07, B1745-12
			1156+314	5.3	B1133+16
			1311-222	16.7	B1325-49
			1021+219	5.7	B0950+08
			2137-207	7.9	J2144-3933
			02/03/2014	3C286	26.4
1924+334	6.5	B1839+09, B1842+14, B1907+10, B1914+09, B1915+13, B1918+19, B1929+10			

Table 5 *continued on next page*

Table 5 (*continued*)

Date	Flux Cal	Flux (Jy)	Phase Cal	Flux (Jy)	Calibrated PSR
			1625-311	3.1	J1557-4258, B1700-32, J1705-3423, B1730-37
09/03/2014	3C48	43.9	0025-260	24.7	J2346-0609
			0116-208	11.5	B0148-06
			2251+188	7.9	B2315+21
			1924+334	6.5	B1915+13, J1919+0134, B1929+10
			0521+166	15.5	B0656+14
			1021+219	6.1	B0950+08
			0837-198	12.7	B0740-28, B0844-35
19/03/2014	3C353	153.4	1830-360	20.7	J1705-3423, B1706-44, B1737-39, B1813-36, B1820-31
			2137-207	8.7	B1929+10, B2045-16
			1822-096	3.6	B1831-04, B1839-04, B1844-04, J1843-0000
			1625-311	3.3	J1700-3312, B1747-46
			1021+219	6.1	B0950+08
27/03/2014	3C147	54.0	0318+164	8.4	B0301+19
28/03/2014	3C286	26.4	1830-360	19.9	B1820-31
			1822-096	3.8	B1758-03, B1804-08, J1808-0813, B1818-04, J1823-0154
			1510-057	7.8	J1603-2531
30/03/2014	3C286	26.4	1830-360	20.5	J1648-3256, B1749-28, J1750-3503, B1754-24 B1758-29, B1813-26, J1817-3837
			1822-096	3.6	B1842+14, B1929+10
			1021+219	6.1	B0950+08
31/05/2014	3C286	26.4	1822-096	3.8	B1819-22, B1846-06, B1929+10
			1830-360	21.0	B1730-22, B1742-30
	3C48	43.9			
21/06/2014	3C48	43.9	1822-096	3.6	B1845-01, B1846-06, J1852-2610, B1929+10
			1924+334	6.5	B1914+09, B1917+00
			2225-049	16.8	B2315+21, J2346-0609
28/06/2014	3C48	43.9	0116-208	12.1	B0203-40
			0323+055	7.3	B0301+19

Table 5 *continued on next page*

Table 5 (*continued*)

Date	Flux Cal	Flux (Jy)	Phase Cal	Flux (Jy)	Calibrated PSR
			1021+219	6.1	B0919+06, B0950+08
			0521+166	15.7	B0656+14
			0837-198	11.4	B0727-18, B0736-40, B0844-35, B0942-13
			1033-343	4.8	J0905-5127
12/07/2014	3C286	26.4	1822-096	3.5	B1737+13, B1738-08, J1835-1106, B1857-26
			1924+334	6.6	B1821+05, J1835-1020, B1907+03, B1929+10
	3C48	43.9	1924+334	6.6	B1944+17
27/07/2014	3C286	26.4			
			1822-096	3.6	B1754-24, B1839-04, J1843-0000, J1848-1414, J1901-0906, B1929+10
			1924+334	6.6	B1944+17
			2251+188	7.8	B2303+30, B2310+42
	3C48	43.9			
<u>610 MHz Observations</u>					
09/02/2014	3C147	39.0	0521+166	13.7	B0523+11, B0540+23, B0611+22, B0626+24, B0656+14
			0521-207	4.4	B0450-18
			0116-208	7.9	B0031-07, J0134-2937, B0149-16
			1924+334	6.3	B1929+10
			2219-279	4.4	J2144-3933
			1830-360	15.8	B1857-26
10/02/2014	3C286	21.7	2047-026	4.2	B1911-04, B2003-08, B2043-04
			1924+334	6.3	B1929+10
			1822-096	6.5	B1718-32, B1719-37, B1742-30
			1154-350	9.5	B1114-41
			1033-343	3.4	J1034-3224
			0804+102	3.5	B0834+06
			0837-198	5.8	B0844-35, B0818-41
			1021+219	3.0	B1133+16
26/02/2014	3C286	21.7	1822-096	6.7	B1737+13, B1821+05, B1839+09, B1929+10
			1924+334	6.3	B1907+10, B1914+09, B1915+13, B1918+19, B1929+10
			1625-311	2.5	B1524-39, J1549-4848, B1552-31
			1330+251	8.2	B1237+25

Table 5 *continued on next page*

Table 5 (*continued*)

Date	Flux Cal	Flux (Jy)	Phase Cal	Flux (Jy)	Calibrated PSR
05/03/2014	3C286	21.7	1021+219	3.1	B0950+08
			1311-222	8.9	B1254-10, B1325-49
			1625-311	2.3	B1504-43, J1557-4258
			1822-096	6.5	B1907+03, B1917+00, B1929+10
			1830-360	16.1	B1737-39
07/03/2014	3C286	21.7	1021+219	3.0	B0950+08
			1510-057	3.4	B1642-03
			1625-311	2.4	J1625-4048, B1717-29, B1730-22
			1822-096	6.5	J1835-1020, J1835-1106, B1842+14, J1848-1414, J1901-0906, B1929+10
			1830-360	16.1	B1700-32, J1705-3423, J1727-2739, B1736-29
20/03/2014	3C48	30.1	2137-207	7.0	B1929+10, B2045-16
			1822-096	6.2	B1831-04, B1839-04, J1843-0000, B1844-04, B1845-01, B1929+10
			1830-360	16.5	B1706-44, B1727-47, B1730-37, B1747-46
			1625-311	2.2	J1648-3256, J1700-3312
			1021+219	3.0	B0919+06, B0950+08
23/03/2014	3C286	21.7	1822-096	6.3	B1738-08, B1758-03, B1804-08, J1808-0813, B1820-31, B1929+10
			1625-311	2.4	B1600-49
	3C48	30.1	2219-279	4.7	B1929+10
			0025-260	14.5	B2327-20, J2346-0609
			0116-208	8.2	B0148-06, B0203-40
			0318+164	9.4	B0301+19
			0706-231	6.1	B0628-28, B0727-18, B0740-28, B0756-15
			1021+219	3.0	B0950+08
27/03/2014	3C48	30.1	1924+334	6.2	B1919+21, B1944+17
			1822-096	6.8	J1817-3837, B1818-04, B1819-22, J1823-0154, B1929+10
			1625-311	2.5	J1603-2531, B1749-28, J1750-3503, B1754-24
			2251+188	4.0	B2315+21
			1830-360	16.1	B1758-29, B1813-26

B. MODE CHANGING IN PULSARS

In this section we present the average profiles of different modes in the 12 pulsars that show the mode changing behaviour.

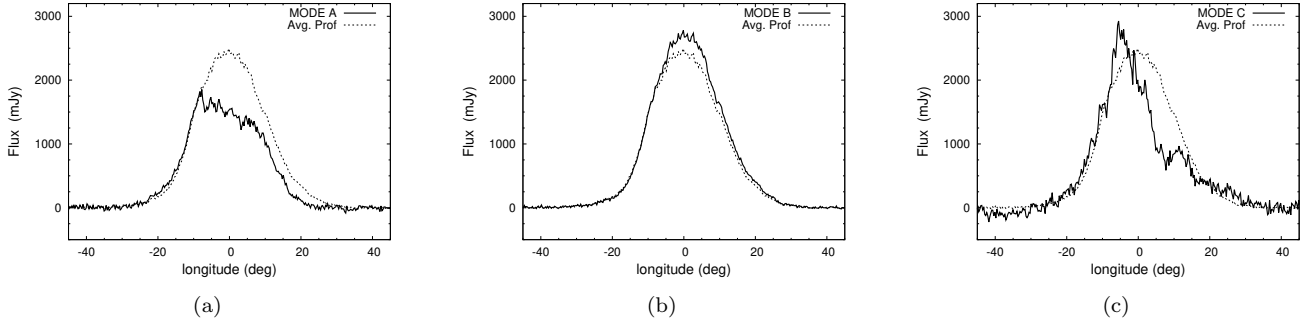


Figure 7. The average profiles in PSR B0031-07 at 325 MHz, (a) Mode A, (b) Mode B and (c) Mode C.

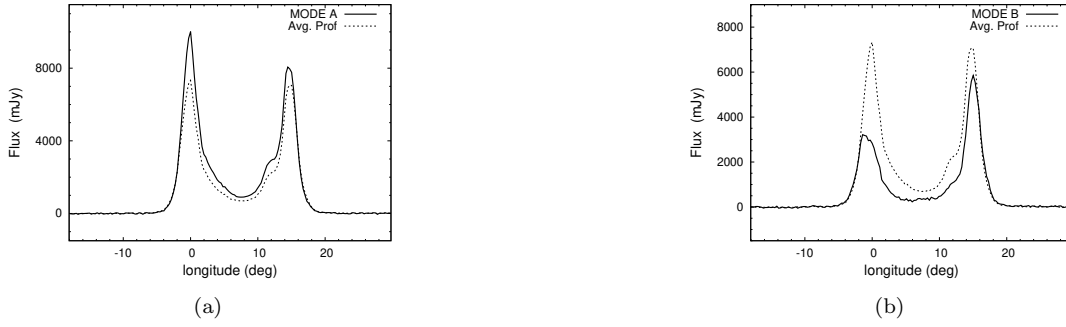


Figure 8. The average profiles in PSR B0525+21 at 325 MHz, (a) Mode A and (b) Mode B.

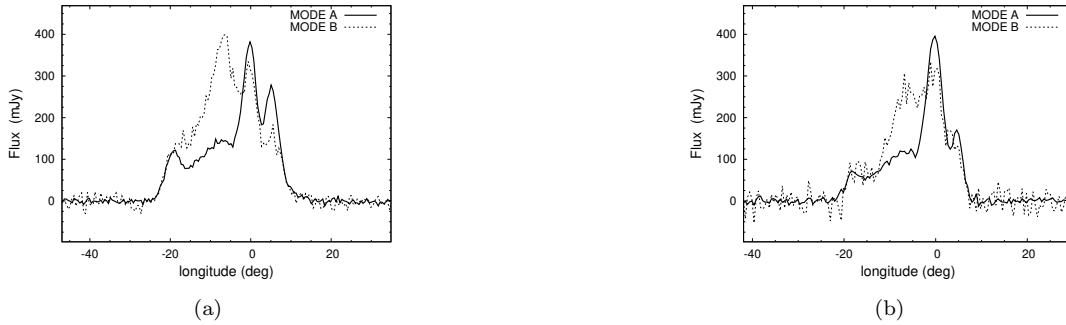


Figure 9. The average profiles of the emission modes in PSR B0844-35, (a) 325 MHz and (b) 610 MHz.

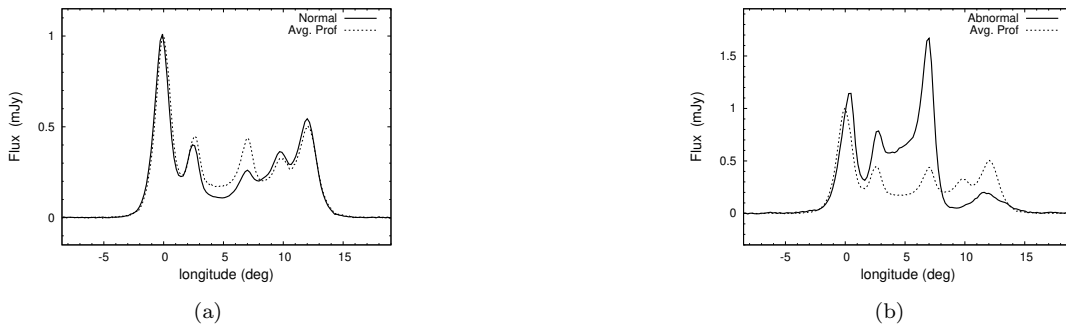


Figure 10. The average profiles of the emission modes in PSR B1237+25 at 325 MHz, (a) Normal mode and (b) Abnormal mode.

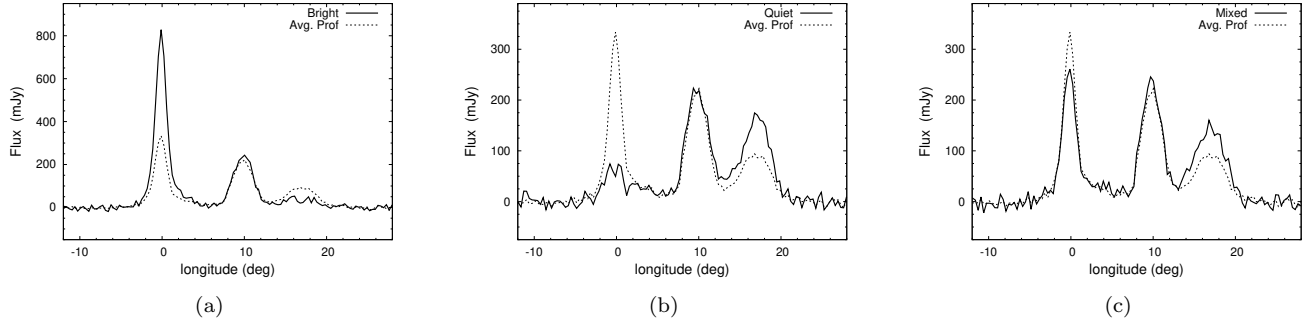


Figure 11. The average profiles in PSR J1625–4048 at 610 MHz, (a) Bright mode, (b) Quiet mode, and (c) Mixed Mode.

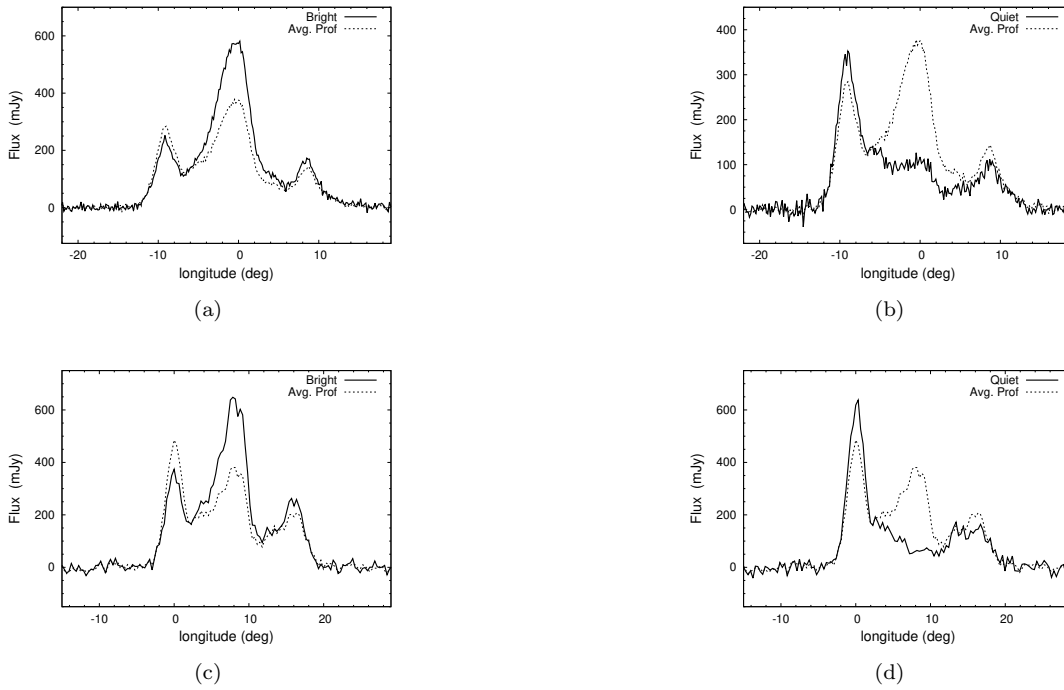


Figure 12. The average profiles in PSR B1758–29, (a) Bright mode at 325 MHz, (b) Quiet mode at 325 MHz, (c) Bright mode at 610 MHz and (d) Quiet mode at 610 MHz.

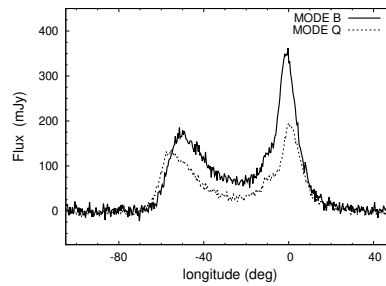


Figure 13. The average profiles of PSR B1839–04 at 610 MHz during the Bright and Quiet modes.

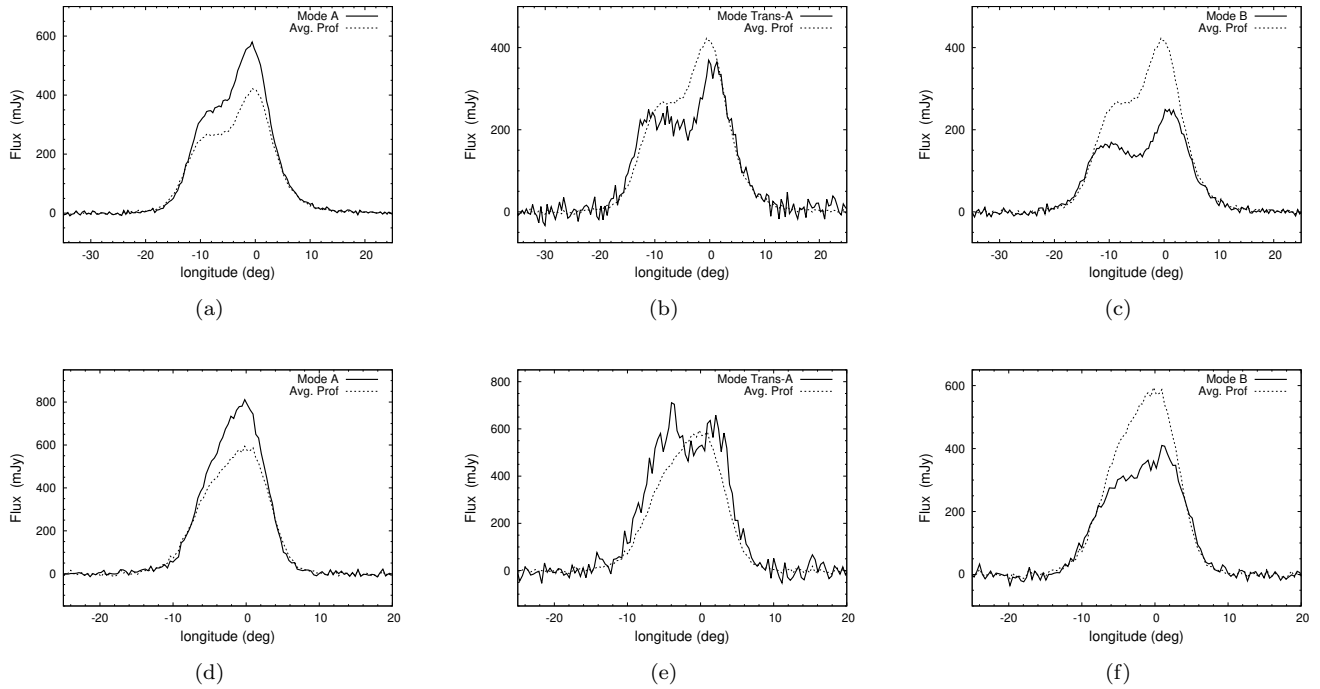


Figure 14. The average profiles in PSR B1819-22, (a) Mode A at 325 MHz, (b) Mode A-Trans at 325 MHz, (c) Mode B at 325 MHz, (d) Mode A at 610 MHz, (e) Mode A-Trans at 610 MHz, and (f) Mode B at 610 MHz.

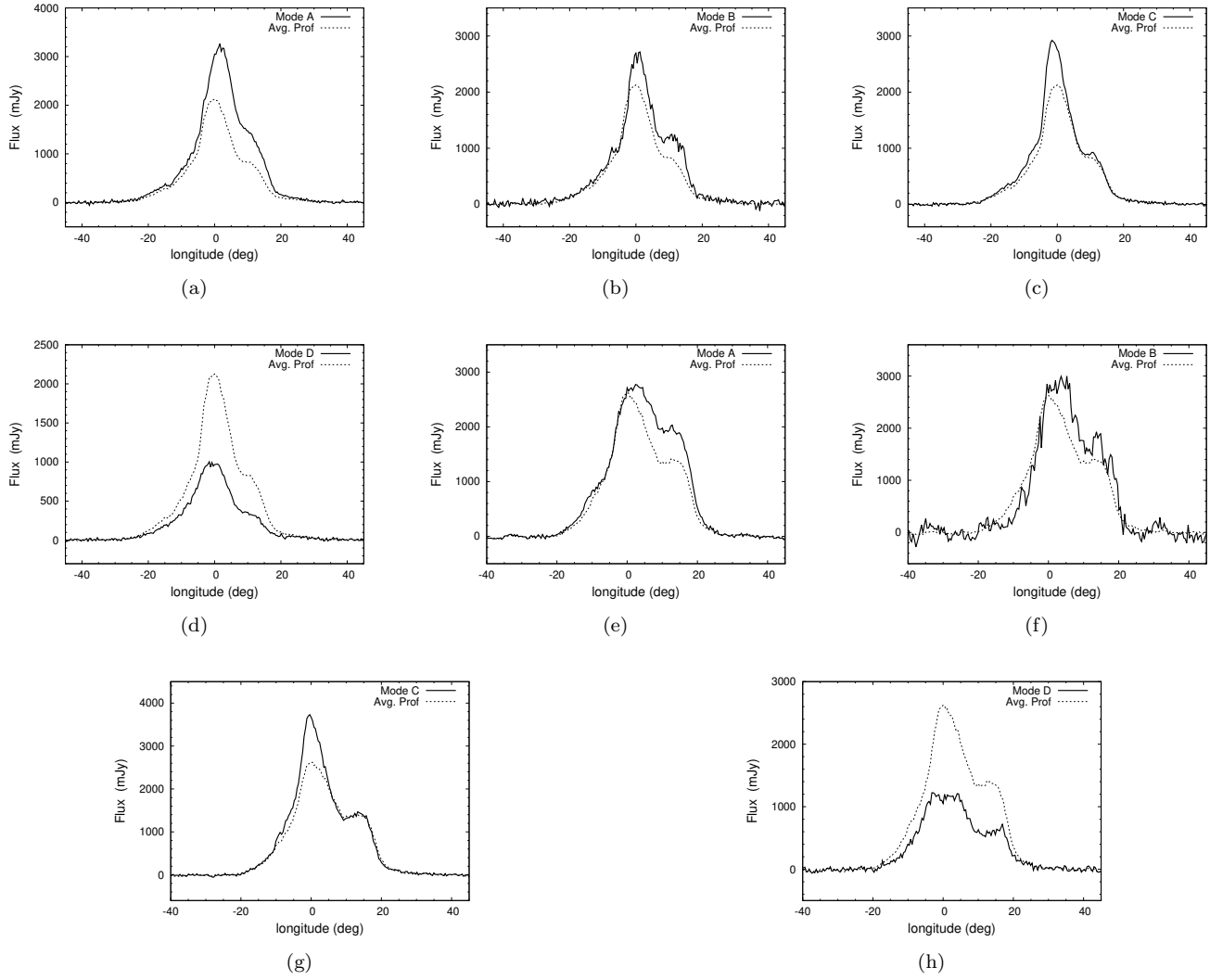


Figure 15. The average profiles in PSR B1944+17, (a) Mode A at 325 MHz, (b) Mode B at 325 MHz, (c) Mode C at 325 MHz, (d) Mode D at 325 MHz, (e) Mode A at 610 MHz, (f) Mode B at 610 MHz, (g) Mode C at 610 MHz, and (h) Mode D at 610 MHz.

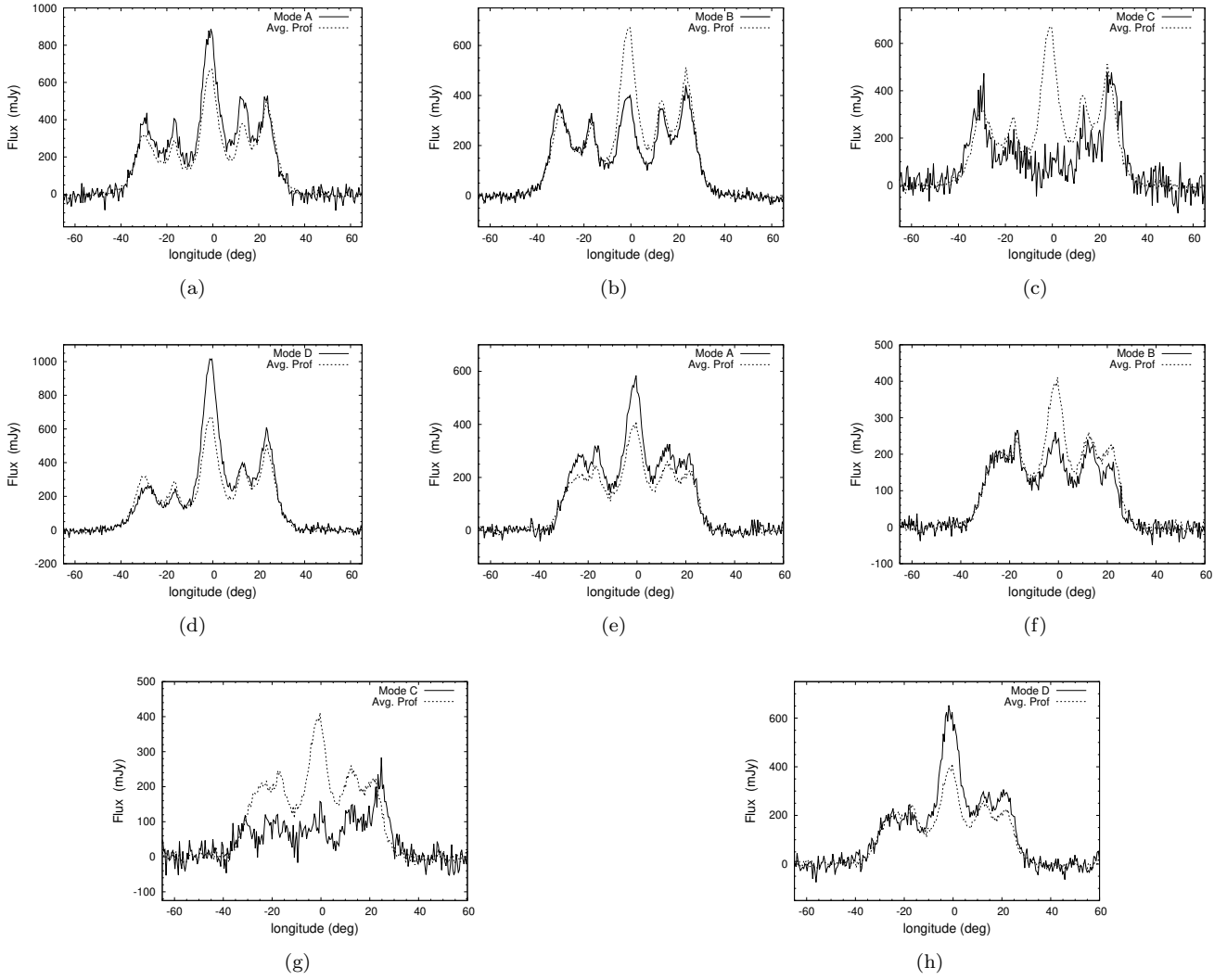


Figure 16. The average profiles in PSR B2003-08, (a) Mode A at 325 MHz, (b) Mode B at 325 MHz, (c) Mode C at 325 MHz, (d) Mode D at 325 MHz, (e) Mode A at 610 MHz, (f) Mode B at 610 MHz, (g) Mode C at 610 MHz, and (h) Mode D at 610 MHz.

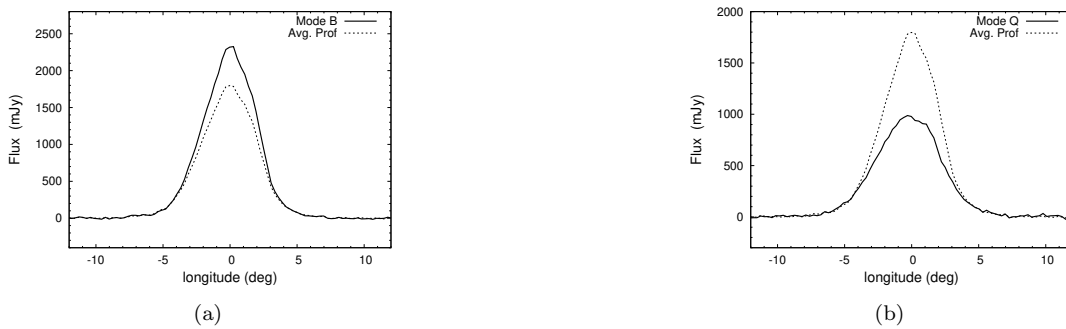


Figure 17. The average profiles of PSR B2303+30 at 325 MHz during the (a) Bright and (b) Quiet modes.